

Article

New Multifunctional Agents for Potential Alzheimer's Disease Treatment Based on Tacrine Conjugates with 2-Arylhydrazinylidene-1,3-Diketones

Natalia A. Elkina ¹, Maria V. Grishchenko ¹, Evgeny V. Shchegolkov ¹, Galina F. Makhaeva ², Nadezhda V. Kovaleva ², Elena V. Rudakova ², Natalia P. Boltneva ², Sofya V. Lushchekina ^{2,3}, Tatiana Y. Astakhova ³, Eugene V. Radchenko ^{2,4}, Vladimir A. Palyulin ^{2,4}, Ekaterina F. Zhilina ¹, Anastasiya N. Perminova ¹, Luka S. Lapshin ¹, Yanina V. Burgart ¹, Victor I. Saloutin ¹ and Rudy J. Richardson ^{5,6,7,8,*}

- ¹ Postovsky Institute of Organic Synthesis, Urals Branch of Russian Academy of Sciences, Yekaterinburg 620990, Russia
² Institute of Physiologically Active Compounds at Federal Research Center of Problems of Chemical Physics and Medicinal Chemistry, Russian Academy of Sciences, Chernogolovka 142432, Russia
³ Emanuel Institute of Biochemical Physics Russian Academy of Sciences, Moscow 119334, Russia
⁴ Department of Chemistry, Lomonosov Moscow State University, Moscow 119991, Russia
⁵ Department of Environmental Health Sciences, University of Michigan, Ann Arbor, MI 48109, USA
⁶ Department of Neurology, University of Michigan, Ann Arbor, MI 48109, USA
⁷ Center of Computational Medicine and Bioinformatics, University of Michigan, Ann Arbor, MI 48109, USA
⁸ Michigan Institute for Computational Discovery and Engineering, University of Michigan, Ann Arbor, MI 48109, USA
* Correspondence: rjrich@umich.edu; Tel.: +1-734-936-0769



Citation: Elkina, N.A.; Grishchenko, M.V.; Shchegolkov, E.V.; Makhaeva, G.F.; Kovaleva, N.V.; Rudakova, E.V.; Boltneva, N.P.; Lushchekina, S.V.; Astakhova, T.Y.; Radchenko, E.V.; et al. New Multifunctional Agents for Potential Alzheimer's Disease Treatment Based on Tacrine Conjugates with 2-Arylhydrazinylidene-1,3-Diketones. *Biomolecules* **2022**, *12*, 1551. <https://doi.org/10.3390/biom12111551>

Academic Editor: Vladimir N. Uversky

Received: 21 September 2022

Accepted: 17 October 2022

Published: 24 October 2022

Publisher's Note: MDPI stays neutral with regard to jurisdictional claims in published maps and institutional affiliations.



Copyright: © 2022 by the authors. Licensee MDPI, Basel, Switzerland. This article is an open access article distributed under the terms and conditions of the Creative Commons Attribution (CC BY) license (<https://creativecommons.org/licenses/by/4.0/>).

Abstract: Alzheimer's disease (AD) is considered a modern epidemic because of its increasing prevalence worldwide and serious medico-social consequences, including the economic burden of treatment and patient care. The development of new effective therapeutic agents for AD is one of the most urgent and challenging tasks. To address this need, we used an aminoalkylene linker to combine the well-known anticholinesterase drug tacrine with antioxidant 2-tolylhydrazinylidene-1,3-diketones to create 3 groups of hybrid compounds as new multifunctional agents with the potential for AD treatment. Lead compounds of the new conjugates effectively inhibited acetylcholinesterase (AChE, IC₅₀ 0.24–0.34 μM) and butyrylcholinesterase (BChE, IC₅₀ 0.036–0.0745 μM), with weak inhibition of off-target carboxylesterase. Anti-AChE activity increased with elongation of the alkylene spacer, in agreement with molecular docking, which showed compounds binding to both the catalytic active site and peripheral anionic site (PAS) of AChE, consistent with mixed type reversible inhibition. PAS binding along with effective propidium displacement suggest the potential of the hybrids to block AChE-induced β-amyloid aggregation, a disease-modifying effect. All of the conjugates demonstrated metal chelating ability for Cu²⁺, Fe²⁺, and Zn²⁺, as well as high antiradical activity in the ABTS test. Non-fluorinated hybrid compounds **6** and **7** also showed Fe³⁺ reducing activity in the FRAP test. Predicted ADMET and physicochemical properties of conjugates indicated good CNS bioavailability and safety parameters acceptable for potential lead compounds at the early stages of anti-AD drug development.

Keywords: Alzheimer's disease; acetylcholinesterase; butyrylcholinesterase; inhibitors; 2-tolylhydrazinylidene-1,3-diketones; tacrine conjugates; propidium displacement; antioxidant activity; biometals; ADMET prediction

1. Introduction

Alzheimer's disease (AD) is the most common form of dementia in old age. It is currently considered a modern epidemic because of its increasing prevalence worldwide

and serious medico-social consequences, including the economic burden of treatment and patient care. This situation is due to a multiplicity of interacting factors including the steadily growing population, increase in life expectancy, duration of the course of the disease, severe disability of patients requiring their hospitalization or expensive in-home care, and the lack of effective therapy [1,2]. Therefore, the development of new effective multifunctional agents that can act simultaneously on several targets thought to be involved in AD pathogenesis is one of the most urgent and important tasks of medicinal chemistry and pharmacology [3].

One of the main characteristics of AD is cholinergic deficiency. A loss of cholinergic innervation in the cerebral cortex of patients with this disorder is an early pathogenic event correlated with cognitive impairment. The severity of dementia has been found to have a positive correlation with the extent of cholinergic loss. This evidence led to the formulation of the “cholinergic hypothesis” and the development of cholinesterase inhibitor therapies for symptomatic improvement in AD patients [4].

Initially, cholinergic therapy for AD was directed toward inhibition of acetylcholinesterase (AChE, EC 3.1.1.7) as the main enzyme that hydrolyzes the neurotransmitter acetylcholine [5]. The therapeutic effect of AChE inhibitors arises from the increased concentrations and duration of action of acetylcholine in cholinergic synapses [6,7]. Butyrylcholinesterase (BChE, EC 3.1.1.8) is also involved in the hydrolysis of acetylcholine and can compensate for some of the functions of AChE, thereby optimizing cholinergic neurotransmission [8–12]. As the disease progresses, the activity of BChE gradually increases while the activity of AChE decreases [12,13]. Consequently, BChE has gained importance as a therapeutic target for reducing cholinergic deficiency [14–16].

Currently, there are no treatments that effectively mitigate the underlying pathogenic mechanisms for AD. Modern therapeutic strategies for AD consist of three cholinesterase inhibitors: donepezil, rivastigmine and galantamine, and the NMDA receptor antagonist memantine. Unfortunately, the effects of these agents are merely palliative. They partially compensate for declining cognitive function but they are not able to stop the development of the neurodegenerative process [7]. Such a small choice of drugs for AD therapy is due to the multifactorial nature of this disease, a realization that has fostered interest in identifying contributing mechanisms and discovering agents capable of attenuating these processes simultaneously [17–19].

One of the best-characterized pathogenic processes of AD is β -amyloid ($A\beta$) protein aggregation and deposition in the brain [20,21]. In addition to the classical function of acetylcholine hydrolysis, AChE has proaggregant properties toward $A\beta$ via participation of the peripheral anionic site (PAS), which interacts with soluble $A\beta$ peptides promoting their aggregation [22,23]. Thus, compounds interacting with the AChE PAS are potential antiaggregating agents [24,25]. Moreover, BChE is also thought to be involved in the formation and/or maturation of $A\beta$ plaques, thereby contributing to AD pathogenesis [26–31]. Therefore, inhibitors of BChE and inhibitors of both cholinesterases are of particular interest from the standpoint of a dual strategy: increasing the concentration of acetylcholine and ameliorating β -amyloid aggregation.

Another important mechanism in many neurodegenerative diseases is oxidative stress, characterized by an imbalance between the formation of reactive oxygen or nitrogen species and their inactivation by antioxidant systems [32–34]. The brain is the most sensitive organ in the body to the damaging effects of free radicals, and this vulnerability increases with age [32,35]. The association between AD and oxidative stress is widely investigated as a potential therapeutic target [36–40], and the design of cholinesterase inhibitors with antioxidant properties is considered a promising direction in the development of multifunctional drugs for AD treatment [41–45].

One of the plausible mechanisms contributing to AD pathogenesis is imbalance of brain homeostasis of certain ions, e.g., Cu^{2+} , Zn^{2+} , and Fe^{2+} . The content of these brain biometals increases 3- to 7-fold during the progression of AD [46]. The accumulation of metals contributes to their binding to $A\beta$, leading to its increased aggregation [47,48].

Moreover, Cu^{2+} and Fe^{2+} support the production of reactive oxygen species and increase of oxidative stress, thus promoting neurotoxicity [49,50]. Therefore, selectively reducing brain concentrations of metals with chelating agents is one of the therapeutic approaches proposed for the treatment of AD [51,52].

Considering the multifactorial nature of AD, a promising therapeutic approach is the development of multitarget drugs having a complex effect on several biological targets responsible for the pathogenesis of this disease [53–57]. One of the design strategies for multitarget drugs is to use a molecular spacer to link together two pharmacophores that are active against two or more different biological targets, and a well-known anticholinesterase drug molecule is often used as one of the pharmacophores [58–62].

Among the anticholinesterases, tacrine was approved in 1993 as the first drug for the treatment of AD [63,64]. However, its serious side effects, such as hepatotoxicity, led to its withdrawal from the market. To improve its activity and reduce its toxicity, new derivatives of tacrine have been designed and synthesized [65,66].

Many studies have been aimed at modifying tacrine by creating hybrid conjugate compounds linked through a spacer with various pharmacophores that promote the interaction of the conjugate inhibitor with both the catalytic active site (CAS) of AChE and its PAS, thus blocking AChE-induced $\text{A}\beta$ aggregation [41,67,68]. In addition, various heterocyclic compounds, e.g., hydroxyquinolines [69] and coumarins [70,71], as well as open-chain fragments such as amino acid derivatives [72,73] and curcumin [74] have been used as a second pharmacophore. These tacrine conjugates combined AChE and BChE inhibition with extra activities, e.g., inhibition of AChE-induced $\text{A}\beta$ aggregation, antioxidant properties, and metal-binding capacity [75–78].

Recently, we found that 2-tolylhydrazinylidene-1,3-diketones have a powerful antioxidant effect exceeding the activity of Trolox by 1.3–1.7 times [79]. Herein, we used these compounds as an antioxidant pharmacophore to create new conjugates by binding them to tacrine through an alkylene linker of various lengths. In the 2-tolylhydrazinylidene-1,3-diketone components **1a–d**, we varied the substituents at the 1,3-diketone fragment including methyl, trifluoromethyl, and phenyl residues. We studied the esterase profile of the synthesized conjugates, i.e., the inhibitory activity against AChE, BChE, and the structurally related enzyme carboxylesterase (CES, EC 3.1.1.1), whose inhibition can result in undesirable drug-drug interactions. In addition, we used quantum mechanics (QM)-assisted molecular docking to explain the observed structure-activity relationships. Moreover, we assessed the efficiency of the new compounds to displace propidium from the AChE PAS as an indicator of their potential ability to block AChE-induced $\text{A}\beta$ aggregation. Furthermore, we determined the antioxidant activity of the conjugates in the ABTS and FRAP tests as well as their metal-chelating ability. Finally, we carried out computational predictions of the ADMET and physicochemical properties of the new conjugates.

2. Materials and Methods

2.1. Chemistry

The solvents (methanol, ethanol, chloroform, methylene chloride, hexane, acetonitrile) were obtained from AO VEKTON (St. Petersburg, Russia). Hexylamine was purchased from Alfa Aesar via Thermo Fisher Scientific (Kandel, Germany). The deuterated solvent CDCl_3 was acquired from SOLVEX LLC (Skolkovo Innovation Center, Moscow, Russia). All solvents, chemicals, and reagents were used without purification. Melting points were determined in open capillaries on a Stuart SMP30 (Bibby Scientific Limited, Staffordshire, UK) melting point apparatus and were uncorrected. The IR spectra were recorded on a PerkinElmer Spectrum Two FT-IR spectrometer (Perkin-Elmer, Waltham, MA, USA) using the frustrated total internal reflection accessory with a diamond crystal. The ^1H and ^{19}F NMR spectra were registered on a Bruker DRX-400 spectrometer (400 or 376 MHz, respectively) or a Bruker Avance^{III} 500 spectrometer (500 or 470 MHz, respectively) (both Bruker, Karlsruhe, Germany). The ^{13}C NMR spectra were recorded on a Bruker Avance^{III} 500 spectrometer (125 MHz). The internal standard was SiMe_4 (for ^1H and ^{13}C NMR

spectra) and C_6F_6 (for ^{19}F NMR spectra, $\delta -162.9$ ppm). The microanalyses (C, H, N) were carried out on a PerkinElmer PE 2400 series II (PerkinElmer, Waltham, MA, USA) elemental analyzer. The column chromatography was performed on Silica gel 60 (0.062–0.2 mm) (Macherey-Nagel GmbH & Co KG, Duren, Germany).

The initial 2-arylhydrazinylidene-1,3-diketones **1a,b** [80], **1c,d** [79] and aminomethylene-tacrines **5a–c** [81] were synthesized by referring to previously published methods.

2.1.1. Synthesis of Compounds **2a–c** (General Procedure)

A mixture of the corresponding 2-arylhydrazinylidene-1,3-diketone **1a,b** (2.3 mmol) and hexylamine (2.3 mmol) was refluxed in dry methanol for 8 h. In the case of (3E)-1,1,1-trifluoro-3-[2-(4-methylphenyl)hydrazinylidene]pentane-2,4-dione **1c**, the reaction was carried out in ethanol at room temperature. Then, the mixture was concentrated on a rotary evaporator. The residue was purified by column chromatography with the appropriate eluent, as specified below.

(3Z)-4-(Hexylamino)-3-[(E)-(4-methylphenyl)diazanyl]pent-3-en-2-one (**2a**). Yield 64%, orange powder, mp 36–37 °C (eluent chloroform: ethanol = 5 : 1, then chloroform). IR: ν 2926 (NH), 1645 (C=O), 1590, 1487, 1436, 1354, 1328 (N–H, C=C, N=N), 1200–1159 (C–F) cm^{-1} . 1H NMR (400 MHz, $CDCl_3$): δ 0.90–0.93, 1.34–1.36, 1.46–1.48, 1.69–1.77 (11H, all m, $HNCH_2(CH_2)_4CH_3$); 2.37, 2.54 (9H, all s, 3 CH_3); 3.45 (2H, unsolv. td, J 6.7, 4.1 Hz, $HNCH_2(CH_2)_4CH_3$); 7.20, 7.43 (4H, both d, J 8.2 Hz); 15.07 (1H, s, NH). ^{13}C NMR (126 MHz, $CDCl_3$): δ 13.99; 16.66; 21.10; 22.54; 26.83; 28.11; 29.29; 31.41; 44.37; 119.34; 129.18; 129.68; 136.29; 148.69; 160.98; 198.52. Anal. calcd. for $C_{18}H_{27}N_3O$. C, 71.72; H, 9.03; N, 13.94. Found: C, 69.96; H, 8.90; N, 13.68.

(3Z)-3-(Hexylamino)-2-[(4-methylphenyl)diazanyl]-1-phenylbut-2-en-1-one (**2b**). Mixture of Z:E-isomers-87:13. Yield 69%, orange powder, mp 54–55 °C (eluent dichloromethane). IR: ν 2924 (NH), 1630 (C=O), 1574, 1514, 1457, 1372, 1335 (N–H, C=C, N=N), 1220–1143 (C–F) cm^{-1} . 1H NMR (400 MHz, $CDCl_3$): δ 0.86–0.87 (3H, m, $HNCH_2(CH_2)_4CH_3$ isomer E); 0.91–0.94 (3H, m, $HNCH_2(CH_2)_4CH_3$ isomer Z); 1.25–1.29, 1.37–1.38, 1.50–1.53, 1.77–1.80 (8H, all m, $HNCH_2(CH_2)_4CH_3$, isomer Z,E); 2.31, 2.55 (6H, both s, 2 CH_3 isomer Z); 2.32, 2.63 (6H, both s, 2 CH_3 isomer E); 7.08–7.10, 7.12–7.13, 7.17–7.18, 7.22–7.23, 7.37–7.47, 7.54–7.56, 7.77–7.79, 7.85–7.87 (9H, all m, Ph and C_6H_4 isomer Z,E); 14.76 (1H, s, NH isomer E); 15.15 (1H, s, NH isomer Z). ^{13}C NMR (125 MHz, $CDCl_3$): δ 14.01; 16.64; 20.93; 21.03; 22.57; 26.91; 29.41; 30.49; 31.45; 45.09; 46.67; 114.18; 115.79; 116.17; 118.71; 119.24; 126.48; 127.19; 127.72; 128.37; 129.18; 129.61; 129.81; 129.95; 130.13; 130.21; 130.32; 131.80; 135.64; 135.96; 138.67; 139.29; 141.32; 148.14; 162.32; 192.21; 193.86. Anal. calcd. for $C_{23}H_{29}N_3O$. C, 76.00; H, 8.04; N, 11.56. Found: C, 76.05; H, 8.22; N, 11.40.

(3Z)-4-(Hexylamino)-3-[(E)-(4-methylphenyl)diazanyl]-1,1,1-trifluoropent-3-en-2-one (**2c**). Yield 40%, orange powder, mp 70–72 °C (eluent chloroform, then hexane:chloroform = 1:1). IR: ν 3258 (NH), 1670 (C=O), 1591, 1558, 1511, 1459, 1365 (N–H, C=C, N=N), 1185–1148 (C–F) cm^{-1} . 1H NMR (500 MHz, $CDCl_3$): δ 0.91–0.94, 1.34–1.38, 1.46–1.50, 1.73–1.78 (11H, all m, $HNCH_2(CH_2)_4CH_3$); 2.38, 2.62 (6H, both s, 2 CH_3); 3.50 (2H, unsolv. td, J 6.8, 5.2 Hz, $HNCH_2(CH_2)_4CH_3$); 7.22, 7.52 (4H, both d, J 8.3 Hz); 14.73 (1H, s, NH). ^{13}C NMR (125 MHz, $CDCl_3$): δ 13.96; 16.32; 21.21; 22.50; 26.64; 28.81; 31.29; 41.88; 118.61 (q, J 292.2 Hz, CF_3); 120.79; 123.23; 129.75; 138.19; 149.50; 164.11; 177.63 (q, J 30.4 Hz, $C-CF_3$). ^{19}F NMR (470 MHz, $CDCl_3$): δ 92.78 (s, CF_3). Anal. calcd. for $C_{18}H_{24}F_3N_3O$. C, 60.83; H, 6.81; N, 10.82. Found: C, 60.66; H, 6.94; N, 11.96.

2.1.2. Synthesis of Compounds **6a–c**, **7a–c**, **8a–c** (General Procedure)

A mixture of 1,1,1-trifluoro-3-[2-(4-methylphenyl)hydrazinylidene]pentane-2,4-dione **1c** (1 mmol) and the corresponding N-(1,2,3,4-tetrahydroacridin-9-yl)alkyldiamine **5a–c** (1 mmol) in 30 mL of dry methylene chloride was stirred at room temperature for 30 min. Then 10 mL of dry methanol was added and the mixture was refluxed for 5 h. In the case of 3-[2-(4-methylphenyl)hydrazinylidene]pentane-2,4-dione **1a** and 2-[2-(4-methylphenyl)hydrazinylidene]-1-phenylbutane-1,3-dione **1b**, the reaction was carried out by refluxing in dry methanol for

8 h. Then the reaction mixture was cooled to room temperature, concentrated on a rotary evaporator, and purified by column chromatography; eluent: dichloromethane:ethanol = 20:1.

(3Z)-3-[(E)-(4-Methylphenyl)diazanyl]-4-((2-[(1,2,3,4-tetrahydroacridin-9-yl)amino]butyl)-amino)pent-3-en-2-one (**6a**). Yield 65%, yellow oil. IR: ν 2928 (NH), 1642 (C=O), 1581, 1562, 1499, 1415, 1352 (N–H, C=C, N=N). ^1H NMR (500 MHz, CDCl_3): δ 1.85–1.88 (8H, m, C^3H_2 , C^4H_2 acridine and $\text{HNCH}_2(\text{CH}_2)_2\text{CH}_2\text{NH}$); 2.35, 2.48, 2.53 (3H, all s, 3 CH_3); 2.67, 3.06 (4H, both t, J 5.8 Hz, C^1H_2 , C^2H_2 acridine); 3.48–3.49, 3.56 (4H, both m, $\text{HNCH}_2(\text{CH}_2)_2\text{CH}_2\text{NH}$); 4.02 (1H, br. s, NH tacrine); 7.13, 7.35 (4H, both d, J 8.2 Hz, $\text{C}_6\text{H}_4\text{CH}_3$); 7.32–7.34, 7.54–7.57, 7.92–7.95 (4H, all m, CH_{Ar}); 15.24 (1H, s, NH). ^{13}C NMR (125 MHz, CDCl_3): δ 16.90; 21.04; 22.60; 22.90; 24.79; 27.10; 27.84; 29.42; 33.72; 44.86; 48.87; 116.32; 118.60; 120.17; 122.51; 123.94; 128.51; 129.79; 130.01; 130.17; 136.05; 147.02; 147.22; 150.49; 158.29; 161.93; 198.41. Anal. calcd. for $\text{C}_{29}\text{H}_{35}\text{N}_5\text{O}$. C, 74.17; H, 7.51; N, 14.91. Found: C, 74.27; H, 7.69; N, 14.73.

(3Z)-3-[(E)-(4-Methylphenyl)diazanyl]-4-((2-[(1,2,3,4-tetrahydroacridin-9-yl)amino]hexyl)-amino)pent-3-en-2-one (**6b**). Yield 55%, yellow oil. IR: ν 2933 (NH), 1647 (C=O), 1642 (C=O), 1574, 1499, 1419, 1353 (N–H, C=C, N=N). ^1H NMR (500 MHz, CDCl_3): δ 1.49–1.50, 1.69–1.74, 1.90–1.91 (12H, all m, C^3H_2 , C^4H_2 acridine and $\text{HNCH}_2(\text{CH}_2)_4\text{CH}_2\text{NH}$); 2.35, 2.52, 2.53 (9H, all s, 3 CH_3); 2.69, 3.07 (4H, both t, J 5.5 Hz, C^1H_2 , C^2H_2 acridine); 3.43 (2H, td, J 6.6, 4.0 Hz, HNCH_2); 3.49 (2H, t, J 7.1 Hz, CH_2NH tacrine); 3.97 (1H, br. s, NH tacrine); 7.16, 7.40 (4H, both d, J 8.1 Hz, $\text{C}_6\text{H}_4\text{CH}_3$); 7.31–7.34, 7.53–7.57, 7.92–7.94 (4H, all m, CH_{Ar}); 15.12 (1H, s, NH). ^{13}C NMR (125 MHz, CDCl_3): δ 16.72; 21.05; 22.69; 22.99; 24.77; 26.63; 26.98; 29.32; 31.61; 33.84; 44.47; 49.26; 115.93; 119.03; 120.14; 122.66; 123.71; 128.39; 128.57; 129.51; 129.70; 136.21; 147.18; 148.16; 150.70; 158.26; 161.26; 198.43. Anal. calcd. for $\text{C}_{31}\text{H}_{39}\text{N}_5\text{O}$. C, 74.81; H, 7.90; N, 14.07. Found: C, 74.38; H, 8.24; N, 13.88.

(3Z)-3-[(E)-(4-Methylphenyl)diazanyl]-4-((2-[(1,2,3,4-tetrahydroacridin-9-yl)amino]octyl)-amino)pent-3-en-2-one (**6c**). Yield 45%, yellow oil. IR: ν 2926 (NH), 1635 (C=O), 1583, 1516, 1456, 1415, 1353 (N–H, C=C, N=N). ^1H NMR (500 MHz, CDCl_3): δ 1.41–1.47, 1.74–1.80, 1.88–1.93, 1.91–1.92 (16H, all m, C^3H_2 , C^4H_2 acridine and $\text{HNCH}_2(\text{CH}_2)_6\text{CH}_2\text{NH}$); 2.33, 2.53 (9H, both s, 3 CH_3); 2.59, 3.28 (4H, both t, J 5.3 Hz, C^1H_2 , C^2H_2 acridine); 3.46, 3.80 (4H, both br.s, $\text{HNCH}_2(\text{CH}_2)_6\text{CH}_2\text{NH}$); 5.27 (1H, br. s, NH tacrine); 7.17, 7.41 (4H, both d, J 8.0 Hz, $\text{C}_6\text{H}_4\text{CH}_3$); 7.41–7.43, 7.66–7.69, 8.10–8.11, 8.43–8.44 (4H, all m, CH_{Ar}); 15.09 (1H, s, NH). ^{13}C NMR (125 MHz, CDCl_3): δ 16.70; 21.07; 21.22; 22.19; 23.92; 26.63; 26.96; 28.06; 29.01; 29.09; 29.25; 29.95; 31.26; 44.35; 48.77; 112.13; 116.21; 117.01; 119.19; 123.25; 123.75; 124.64; 129.29; 129.65; 130.17; 131.10; 136.28; 148.45; 154.01; 161.11; 198.48. Anal. calcd. for $\text{C}_{33}\text{H}_{43}\text{N}_5\text{O}$. C, 75.39; H, 8.24; N, 13.32. Found: C, 75.43; H, 8.17; N, 13.69.

(2Z)-2-[(E)-(4-Methylphenyl)diazanyl]-1-phenyl-3-((2-[(1,2,3,4-tetrahydroacridin-9-yl)amino]butyl)amino)but-2-en-1-one (**7a**). Yield 68%, yellow oil. IR: ν 2930 (NH), 1626 (C=O), 1578, 1499, 1416, 1335 (N–H, C=C, N=N). ^1H NMR (500 MHz, CDCl_3): δ 1.88–1.91 (8H, m, C^3H_2 , C^4H_2 acridine and $\text{HNCH}_2(\text{CH}_2)_2\text{CH}_2\text{NH}$); 2.30, 2.48 (6H, both s, 2 CH_3); 2.70, 3.08 (4H, both t, J 5.8 Hz, C^1H_2 , C^2H_2 acridine); 3.57–3.61 (4H, m, $\text{HNCH}_2(\text{CH}_2)_2\text{CH}_2\text{NH}$); 3.99 (1H, br. s, NH tacrine); 7.03, 7.10 (4H, both d, J 8.1 Hz, $\text{C}_6\text{H}_4\text{CH}_3$); 7.34–7.37, 7.39–7.42, 7.74–7.48 (5H, all m, C_6H_5); 7.56–7.59, 7.81–7.82, 7.94–7.96 (4H, all m, CH_{Ar}); 15.37 (1H, s, NH). ^{13}C NMR (125 MHz, CDCl_3): δ 16.91; 20.99; 22.68; 22.94; 24.83; 27.23; 29.52; 33.96; 45.69; 48.97; 116.51; 118.40; 120.33; 122.51; 123.87; 127.29; 128.36; 128.80; 129.72 (2C); 130.02; 130.26; 130.68; 135.65; 140.67; 146.56; 147.37; 150.33; 158.56; 163.26; 193.60. Anal. calcd. for $\text{C}_{34}\text{H}_{37}\text{N}_5\text{O}$. C, 76.80; H, 7.01; N, 13.17. Found: C, 76.65; H, 7.15; N, 13.29.

(2Z)-2-[(E)-(4-Methylphenyl)diazanyl]-1-phenyl-3-((2-[(1,2,3,4-tetrahydroacridin-9-yl)amino]hexyl)amino)but-2-en-1-one (**7b**). Yield 57%, yellow oil. IR: ν 2930, 2858 (NH), 1626 (C=O), 1578, 1499, 1366, 1335 (N–H, C=C, N=N). ^1H NMR (500 MHz, CDCl_3): δ 1.51–1.55, 1.69–1.75, 1.76–1.80, 1.90–1.91 (12H, all m, C^3H_2 , C^4H_2 acridine and $\text{HNCH}_2(\text{CH}_2)_4\text{CH}_2\text{NH}$); 2.29, 2.51 (6H, both s, 2 CH_3); 2.69, 3.07 (4H, both t, J 5.7 Hz, C^1H_2 , C^2H_2 acridine); 3.48–3.53 (4H, m, $\text{HNCH}_2(\text{CH}_2)_4\text{CH}_2\text{NH}$); 4.02 (1H, br. s, NH tacrine); 7.05, 7.14 (4H, both d, J 8.1 Hz, $\text{C}_6\text{H}_4\text{CH}_3$); 7.32–7.35, 7.37–7.42; 7.54–7.57 (5H, all m, C_6H_5); 7.54–7.57, 7.78–7.79, 7.93–7.95 (4H, all m, CH_{Ar}); 15.21 (1H, s, NH). ^{13}C NMR (125 MHz, CDCl_3): δ 16.72; 21.00; 22.64;

22.95; 24.74; 26.66; 27.04; 29.42; 31.68; 33.74; 45.19; 49.27; 115.83; 118.91; 120.05; 122.71; 123.72; 127.23 (2C); 128.45; 129.46; 129.63; 129.84; 130.21; 130.48; 135.90; 141.04; 147.05; 147.59; 150.78; 158.17; 162.60; 193.76. Anal. calcd. for C₃₆H₄₁N₅O. C, 77.25; H, 7.38; N, 12.51. Found: C, 77.55; H, 7.68; N, 12.23.

(2Z)-2-[(E)-(4-Methylphenyl)diazenyl]-1-phenyl-3-((2-[(1,2,3,4-tetrahydroacridin-9-yl)amino]octyl)amino)but-2-en-1-one (7c). Yield 47%, yellow oil. IR: ν 2927, 2855 (NH), 1628 (C=O), 1576, 1514, 1501, 1366, 1335 (N–H, C=C, N=N). ¹H NMR (500 MHz, CDCl₃): δ 1.41–1.51, 1.68–1.72, 1.74–1.79, 1.90–1.91 (16H, all m, C³H₂, C⁴H₂ acridine and HNCH₂(CH₂)₆CH₂NH); 2.28, 2.53 (6H, both s, 2CH₃); 2.65, 3.12 (4H, both t, *J* 5.3 Hz, C¹H₂, C²H₂ acridine); 3.51 (2H, td, *J* 6.7, 4.1 Hz, HNCH₂); 3.56 (2H, t, *J* 7.1 Hz, CH₂NH tacrine); 3.97 (1H, br s, NH tacrine); 4.27 (1H, br. s, NH tacrine); 7.07, 7.16 (4H, both d, *J* 8.1 Hz, C₆H₄CH₃); 7.34–7.41, 7.44–7.46 (5H, all m, C₆H₅); 7.56–7.60, 7.77–7.79, 7.97–7.99 (4H, all m, CH_{Ar}); 15.17 (1H, s, NH). ¹³C NMR (125 MHz, CDCl₃): δ 16.65; 20.99; 22.24; 22.73; 24.44; 26.76; 29.09; 29.19; 29.35; 31.56; 45.07; 49.21; 114.66; 119.10; 123.08; 123.88; 126.94; 127.20; 128.35; 129.14; 129.26; 129.58; 130.17; 130.28; 130.40; 135.95; 139.30; 141.15; 145.50; 147.92; 151.73; 156.82; 162.40; 193.80. Anal. calcd. for C₃₈H₄₅N₅O. C, 77.65; H, 7.72; N, 11.91. Found: C, 77.45; H, 7.92; N, 11.74.

(3Z)-3-[(E)-(4-Methylphenyl)diazenyl]-4-((2-[(1,2,3,4-tetrahydroacridin-9-yl)amino]butyl)amino)-1,1,1-trifluoropent-3-en-2-one (8a). Yield 60%, crystalizing oil. IR: ν 2942, 2868 (NH), 1671 (C=O), 1585, 1562, 1496, 1368 (N–H, C=C, N=N), 1220–1143 (C–F) cm⁻¹. ¹H NMR (500 MHz, CDCl₃): δ 1.85–1.90 (8H, m, C³H₂, C⁴H₂ acridine and HNCH₂(CH₂)₂CH₂NH); 2.37, 2.59 (6H, both s, 2CH₃); 2.69, 3.06 (4H, both t, *J* 6.0 Hz, C¹H₂, C²H₂ acridine); 3.52–3.54 (4H, m, HNCH₂(CH₂)₂CH₂NH); 3.88 (1H, br. s, NH tacrine); 7.17, 7.47 (4H, both d, *J* 8.2 Hz, C₆H₄CH₃); 7.33–7.36, 7.46–7.48, 7.55–7.58; 7.89–7.93 (4H, all m, CH_{Ar}); 14.88 (1H, s, NH). ¹³C NMR (125 MHz, CDCl₃): δ 16.32; 21.20; 22.69; 22.92; 24.86; 26.48; 29.15; 34.01; 43.62; 48.67; 116.87; 118.50 (q, *J* 292.1 Hz, CF₃); 120.44; 120.61; 122.32; 123.41; 123.99; 128.38; 128.94; 129.82; 138.34; 147.43; 149.10; 150.06; 158.71; 164.15; 177.67 (q, *J* 30.4 Hz, C–CF₃). ¹⁹F NMR (470 MHz, CDCl₃): δ 92.68 (s, CF₃). Anal. calcd. for C₂₉H₃₂F₃N₅O. C, 66.52; H, 6.16; N, 13.38. Found: C, 66.30; H, 6.36; N, 13.02.

Crystallographic data for compound 8a. The X-ray studies were performed on an Xcalibur 3 CCD (Oxford Diffraction Ltd., Abingdon, UK) diffractometer with a graphite monochromator, ω scanning with 1° step, λ (MoK α) 0.71073 Å radiation, T 295(2) K. An empirical absorption correction was applied. Using Olex2 [82], the structure was solved with the ShelXT [83] structure solution program using Direct Methods and refined with the ShelXL [84] refinement package using Least Squares minimization. All non-hydrogen atoms were refined in the anisotropic approximation; H-atoms at the C–H bonds were refined in the “rider” model with dependent displacement parameters. An empirical absorption correction was carried out through spherical harmonics, implemented in the SCALE3 ABSPACK scaling algorithm by a program “CrysAlisPro 1.171.41.123a” (Rigaku Oxford Diffraction, 2022).

The suitable orange single crystals of compound **8a** were obtained by slow crystallization from acetonitrile. Main crystallographic data for **8a**: C₂₉H₃₂F₃N₅O, M 523.59, space group P2₁/n, monoclinic, *a* 9.6290(8), *b* 24.6933(16), *c* 11.4045(8) Å; β 103.973(7)°; *V* 2631.4(3) Å³; *Z* 4; *D*_{calc} 1.322 g·cm⁻³; μ 0.097 mm⁻¹; 370 refinement parameters; 22,006 reflections measured, 7024 [R_{int} = 0.0580, R_{sigma} = 0.0626] unique reflections which were used in all calculations. The final R₁ = 0.0843, wR₂ = 0.2237 [I ≥ 2σ (I)], R₁ = 0.1441, wR₂ = 0.2836 [all data]. CCDC 2165596 contains the supplementary crystallographic data for this compound.

(3Z)-3-[(E)-(4-Methylphenyl)diazenyl]-4-((2-[(1,2,3,4-tetrahydroacridin-9-yl)amino]hexyl)amino)-1,1,1-trifluoropent-3-en-2-one (8b). Yield 48%, yellow oil. IR: ν 2931 (NH), 1663 (C=O), 1591, 1562, 1497, 1421, 1382 (N–H, C=C, N=N), 1169–1143 (C–F) cm⁻¹. ¹H NMR (500 MHz, CDCl₃) δ 1.55–1.56, 1.78–1.88 (12H, all m, C³H₂, C⁴H₂ acridine and HNCH₂(CH₂)₄CH₂NH); 2.36, 2.60 (6H, both s, 2CH₃); 2.62, 3.19 (4H, both t, *J* 5.6 Hz, C¹H₂, C²H₂ acridine); 3.52 (2H, td, *J* 6.6, 5.2 Hz, HNCH₂); 3.75 (2H, t, *J* 6.9 Hz, CH₂NH tacrine); 5.07 (1H, br. s, NH tacrine); 7.18, 7.48 (4H, both d, *J* 8.3 Hz, C₆H₄CH₃); 7.35–7.38, 7.60–7.63, 8.04–8.05, 8.26–8.28 (4H,

all m, CH_{Ar}); 14.75 (1H, s, NH). ¹³C NMR (125 MHz, CDCl₃) δ 16.36; 21.20; 21.45; 22.32; 24.23; 26.38; 26.67; 28.75; 29.67; 31.22; 43.70; 48.57; 112.98; 117.64; 118.53 (q, *J* 291.8 Hz, CF₃); 120.68; 123.29; 123.52; 124.09; 124.51; 129.76; 130.56; 138.30; 142.48; 149.34; 153.36; 154.33; 164.16; 177.59 (q, *J* 30.4 Hz, C—CF₃). ¹⁹F NMR (470 MHz, CDCl₃): δ 92.73 (s, CF₃). Anal. calcd. for C₃₁H₃₆F₃N₅O. C, 67.49; H, 6.58; N, 12.70. Found: C, 67.39; H, 6.35; N, 12.42.

(3Z)-3-[(E)-(4-Methylphenyl)diazenyl]-4-((2-[(1,2,3,4-tetrahydroacridin-9-yl)amino]octyl)-amino-1,1,1-trifluoropent-3-en-2-one (8c). Yield 42%, yellow oil. IR: ν 2927 (NH), 1663 (C=O), 1592, 1562, 1498, 1421, 1382 (N—H, C=C, N=N), 1169–1144 (C—F) cm⁻¹. ¹H NMR (500 MHz, CDCl₃) δ 1.38–1.48, 1.63–1.67, 1.72–1.75, 1.91–1.92 (16H, all m, C²H₂, C³H₂ acridine + HNCH₂(CH₂)₆CH₂NH); 2.36, 2.61 (6H, both s, 2CH₃); 2.70, 3.06 (4H, both t, *J* 5.3 Hz, C¹H₂, C⁴H₂ acridine); 3.45–3.51 (4H, m, HNCH₂(CH₂)₆CH₂NH); 3.93 (1H, br. s, NH tacrine); 7.20, 7.50 (4H, both d, *J* 8.2 Hz, C₆H₄CH₃); 7.32–7.35, 7.53–7.56, 7.90–7.94 (4H, all m, CH_{Ar}); 14.73 (1H, s, NNH). ¹³C NMR (125 MHz, CDCl₃): δ 16.34; 21.20; 22.73; 23.01; 24.75; 26.81; 26.86; 28.82; 29.04; 29.19; 31.70; 33.91; 43.81; 49.38; 115.83; 118.57 (q, *J* 292.1 Hz, CF₃); 120.15; 120.76; 122.77; 123.28; 123.61; 128.34; 128.61; 129.75; 138.24; 147.31; 149.46; 150.76; 158.34; 164.11; 177.66 (q, *J* 30.8 Hz, C—CF₃). ¹⁹F NMR (470 MHz, CDCl₃): δ 92.75 (s, CF₃). Anal. calcd. for C₃₃H₄₀F₃N₅O. C, 68.37; H, 6.96; N, 12.08. Found: C, 68.54; H, 7.05; N, 12.13.

2.2. Biological Testing

2.2.1. Enzymatic Assays

AChE, BChE and CES Inhibition

Human erythrocyte AChE, equine serum BChE, porcine liver CES, acetylthiocholine iodide (ATCh), butyrylthiocholine iodide (BTCh), 5,5'-dithio-bis-(2-nitrobenzoic acid) (DTNB), 4-nitrophenyl acetate (4-NPA), tacrine were purchased from Sigma-Aldrich (St. Louis, MO, USA). AChE and BChE activities were measured by the colorimetric method of Ellman (λ 412 nm). The assay solution consisted of 0.1 M K/Na phosphate buffer pH 7.5, 25 °C, 0.33 mM DTNB, 0.02 unit/mL AChE or BChE, and 1 mM substrate (ATCh or BTCh, respectively). Reagent blanks consisted of reaction mixtures without substrates.

The activity of CES was determined spectrophotometrically by the release of 4-nitrophenol at 405 nm in 0.1 M K/Na phosphate buffer pH 8.0, 25 °C. Final enzyme and substrate (4-nitrophenyl acetate) concentrations were 0.02 unit/mL and 1 mM, respectively. Assays were carried out with a blank containing all constituents except porcine CES to assess non-enzymatic hydrolysis. Measurements were performed with a FLUOStar Optima microplate reader (BMG Labtech, Ortenberg, Germany). Compounds were dissolved in DMSO; the incubation mixture contained 2% (*v/v*) solvent. The primary evaluation of the inhibitory activity of the compounds was performed by determining the degree of the enzyme inhibition at a compound concentration of 20 μM. For this, a sample of the corresponding enzyme was incubated with the test compound for 5 min; then the enzyme residual activity was determined. Each experiment was performed in triplicate. Compounds inhibiting the enzyme by more than 30% were then selected for determination of IC₅₀ values (the inhibitor concentration resulting in 50% inhibition of control enzyme activity). Compounds (eight concentrations ranging between 1 × 10⁻¹¹ and 1 × 10⁻⁴ M were used to achieve 20 to 80% inhibition) were incubated with each enzyme for 5 min at 25 °C (for temperature equilibration). Substrate was then added and residual enzyme activity relative to an inhibitor-free control was measured using a FLUOStar Optima microplate reader.

Kinetic Study of AChE and BChE Inhibition. Determination of Inhibition Mechanism and Steady-State Inhibition Constants

Mechanisms of human erythrocyte AChE and equine serum BChE inhibition were assessed via a thorough analysis of enzyme kinetics. Residual activity was measured following 5 min incubation at 25 °C with three increasing concentrations of inhibitor and six decreasing substrate concentrations. Inhibition constants *K_i* (competitive component)

and αK_i (noncompetitive component) were determined by linear regression of $1/V$ versus $1/[S]$ double-reciprocal (Lineweaver–Burk) plots.

2.2.2. Propidium Displacement from *EeAChE* PAS

Propidium iodide, donepezil, and Tris were purchased from Sigma-Aldrich (St. Louis, MO, USA). The ability of the test compounds to competitively displace propidium, a selective ligand of the PAS of AChE, was evaluated by a fluorescence method [85]. *Electrophorus electricus* (*EeAChE*) (electric eel, type VI-S, lyophilized powder, Sigma-Aldrich, St. Louis, MO, USA) was used owing to its high degree of purification, high activity, and lower cost than human AChE (hAChE). The applicability of this enzyme has been substantiated earlier [67]. The fluorescence intensity of propidium iodide bound with AChE increases several times; decreasing fluorescence intensity of the bound propidium in the presence of the test compounds shows their ability to bind to the PAS of AChE. To determine the degree of displacement (% displacement) of propidium from the PAS of AChE, *EeAChE* (final concentration, 7 μM) was incubated with the test compound at a concentration of 20 μM in 1 mM Tris-HCl buffer pH 8.0, 25 °C, for 15 min. Then, propidium iodide solution (final concentration, 8 μM) was added, the samples were incubated for 15 min, and the fluorescence spectrum (530 nm (excitation) and 600 nm (emission)) was taken. Donepezil and tacrine were used as reference compounds. The blank contained propidium iodide of the same concentration in 1 mM Tris-HCl buffer, pH 8.0 at 25 °C. The measurements were carried out in triplicate on a FLUOStar Optima microplate reader (LabTech, Ortenberg, Germany), and the results were calculated by the following formula:

$$\% \text{ Displacement} = 100 - (\text{IF}_{\text{AChE} + \text{Propidium} + \text{inhibitor}} / \text{IF}_{\text{AChE} + \text{Propidium}}) \times 100 \quad (1)$$

where $\text{IF}_{\text{AChE} + \text{Propidium}}$ is the fluorescence intensity of the propidium associated with AChE in the absence of the test compound (taken as 100%), and $\text{IF}_{\text{AChE} + \text{Propidium} + \text{inhibitor}}$ is the fluorescence intensity of the propidium associated with AChE in the presence of the test compound.

2.2.3. ABTS Radical Cation Scavenging Activity Assay

Radical scavenging activity of the compounds was evaluated by the ABTS radical cation ($\text{ABTS}^{\bullet+}$) scavenging assay showing the ability of the compounds to decolorize the $\text{ABTS}^{\bullet+}$ solution [86] with some modifications [87]. Trolox was used as the antioxidant standard; ascorbic acid was used as the comparison compound. All tested compounds and standards were dissolved in DMSO.

ABTS (2,2'-azinobis-(3-ethylbenzothiazoline-6-sulfonic acid)) was purchased from Tokyo Chemical Industry Co., Ltd. (Tokyo, Japan). Potassium persulfate (dipotassium peroxydisulfate), Trolox (6-hydroxy-2,5,7,8-tetramethylchroman-2-carboxylic acid), ascorbic acid, DMSO and HPLC-grade ethanol were obtained from Sigma-Aldrich Chemical Co. (St. Louis, MO, USA). Aqueous solutions were prepared using deionized water.

The solution of $\text{ABTS}^{\bullet+}$ was produced by mixing 7 mM ABTS aqueous solution with 2.45 mM potassium persulfate aqueous solution in equal quantities and allowing them to react for 12–16 h at room temperature in the dark. Radical scavenging capacity of the compounds was analyzed by mixing 10 μL of compound with 240 μL of $\text{ABTS}^{\bullet+}$ working solution in ethanol (100 μM final concentration), and after 1 h of incubation at 30 °C the decrease in absorbance was measured spectrophotometrically at 734 nm using a Bio-Rad xMark microplate UV/VIS spectrophotometer (Bio-Rad, Hercules, CA, USA). The compounds were tested in the concentration range 5×10^{-7} – 1×10^{-4} M. Ethanol blanks were run in each assay. Values were obtained from five replicates of each sample and three independent experiments.

Antioxidant activity was reported as Trolox equivalent antioxidant capacity (TEAC values), consisting of the ratio between the slopes obtained from the linear correlation for concentrations of the tested compounds and Trolox with absorbance of ABTS radical. For the compounds, we also determined IC_{50} values (compound concentration (μM))

required for 50% reduction of the ABTS radical). The calculations were carried out using Origin 6.1 for Windows (OriginLab, Northampton, MA, USA). Results are presented as mean \pm SEM calculated using GraphPad Prism version 6.05 for Windows, GraphPad Software (San Diego, CA, USA).

2.2.4. Ferric Reducing Antioxidant Power (FRAP) Assay

The FRAP (Ferric Reducing Antioxidant Power) assay measures the ability of antioxidants to reduce the ferric 2,4,6-tripyridyl-s-triazine complex $[\text{Fe}(\text{TPTZ})_2]^{3+}$ to the intensely blue-colored ferrous complex $[\text{Fe}(\text{TPTZ})_2]^{2+}$ with an absorption maximum at $\lambda = 593 \text{ nm}$ [88,89]. The reducing ability of a compound is an indicator of its potential antioxidant activity [90].

The ferric reducing ability of the compounds was determined by a previously described method [89] as a microplate-adapted version described in [42]. 2,4,6-tris(pyridin-2-yl)-1,3,5-triazine (TPTZ), $\text{FeCl}_3 \cdot 6\text{H}_2\text{O}$, Trolox, ascorbic acid and DMSO were obtained from Sigma-Aldrich Chemical Co (St. Louis, MO, USA). The FRAP reagent was prepared by mixing acetate buffer (0.3 M, pH 3.6), TPTZ (10 mM in 40 mM HCl) and $\text{FeCl}_3 \cdot 6\text{H}_2\text{O}$ (20 mM in distilled water) in a ratio of 10:1:1 immediately before use. Compounds were dissolved in DMSO and tested in the concentration range of 1×10^{-6} – 1×10^{-4} M. The solvent content in the reaction mixture was 4% (*v/v*). The test compounds (10 μL) were added to the FRAP reagent solution (240 μL) and mixed thoroughly. The reaction was carried out at 37 °C in the dark, the incubation time was 1 h. The absorbance at 600 nm was monitored spectrophotometrically by a FLUOStar OPTIMA microplate reader (BMG Labtech, Germany) at 37 °C. Trolox was used as a standard antioxidant, ascorbic acid as a reference compound. Values were obtained from four replicates of each sample and three independent experiments.

The ferric reducing ability of compounds was expressed as TE units (antioxidant activity in Trolox equivalent) with the values calculated as the ratio of the concentrations of Trolox and the test compound resulting in the same effect.

2.2.5. Metal-chelating Properties of Compounds 6a, 7a and 8a

The complexing studies were made in acetonitrile at 25 °C using a UV-vis spectrophotometer Shimadzu UV-2600 (Shimadzu Corporation, Kyoto, Japan) with wavelength ranging from 190 to 600 nm. Solutions (200 μM in acetonitrile) of the following metals compounds were prepared in volumetric flasks: $\text{FeCl}_2 \cdot 4\text{H}_2\text{O}$ (99%, Acros Organics by Thermo Fisher Scientific (Kandel, Germany)), CuCl_2 (98%, Alfa Aesar by Thermo Fisher Scientific (Kandel, Germany)), or $\text{Zn}(\text{NO}_3)_2 \cdot 6\text{H}_2\text{O}$ (98%, Alfa Aesar by Thermo Fisher Scientific (Kandel, Germany)). Solutions of the test compounds were also prepared in acetonitrile at 400 μM concentrations. To a mixture of 0.5 mL test compound solution (40 μM final concentration) and 3.5 mL acetonitrile, 1 mL of the metal solution (CuCl_2 , $\text{FeCl}_2 \cdot 4\text{H}_2\text{O}$, or $\text{Zn}(\text{NO}_3)_2 \cdot 6\text{H}_2\text{O}$; 40 μM final concentration) was added. The solution was incubated at 25 °C for 30 min and then the absorption spectra were recorded at 25 °C in a 1 cm quartz cell. The control was prepared by mixing 0.5 mL tested compound solution and 4.5 mL acetonitrile.

2.2.6. Molecular Modeling Studies

QM analysis of the Structures

Estimations of pK_a values were performed with the Calculator Plugins of MarvinSketch 21.14.0, ChemAxon (<http://www.chemaxon.com>, accessed on 19 September 2021). Because the pK_a values of the tacrine fragment for all considered compounds was estimated as 8.89, all conjugates were used for all further calculations with a protonated endocyclic nitrogen atom of the tacrine fragment.

For all considered compounds an array of possible tautomers was also generated with the Calculator Plugins of MarvinSketch 21.14.0. A conformational search was performed with TorsiFlex v. 2021.3 [91,92], for all torsions of the hydrazone-diketone fragment, with

connectivity of the mobile hydrogen skipped. The following main parameters of TorsiFlex were used: 10,000 of steps of a stochastic algorithm (increased to 20,000 and 50,000 when an additional search was needed), HF/3-21G for low level and B3LYP/6-31G* for high level calculations.

QM optimization of the generated structures, as well as proton transfer pathway calculations (optimization, transition state (TS) search and intrinsic reaction path calculations (IRC)) were performed with Gaussian 16 [93] using a DFT method (B3LYP/6-31G*).

Molecular Docking

The X-ray structure of human AChE co-crystallized with donepezil (PDB ID 4EY7 [94]) after removal of water molecules and other molecules, and an optimized X-ray structure of human BChE (PDB ID 1POI [95,96]) were used for molecular docking. Structures of the ligands in the most stable configuration after QM optimization were used. Partial atomic charges on ligand atoms were assigned from QM data according to the Löwdin scheme [97].

Molecular docking was performed with AutoDock 4.2.6 software [98]. The grid box for docking included the entire active site gorge of AChE (22.5Å × 22.5Å × 22.5Å grid box dimensions) and BChE (15Å × 20.25Å × 18Å grid box dimensions) with a grid spacing of 0.375 Å. The main Lamarckian Genetic Algorithm (LGA) [99] parameters were 256 runs, 25 × 10⁶ evaluations, 27 × 10⁴ generations, and a population size of 3000.

Figures were prepared with PyMol (www.pymol.org, accessed on 21 July 2016).

2.2.7. Prediction of ADMET and Physicochemical Profiles

Lipophilicity (LogP_{ow}) and aqueous solubility (pS) were estimated by the ALogPS 3.0 neural network model implemented in the OCHEM platform [100]. Human intestinal absorption (HIA) [101], blood–brain barrier distribution/permeability (LogBB) [102,103], and hERG-mediated cardiac toxicity risk (channel affinity pK_i and inhibitory activity pIC₅₀) [104] were estimated using the integrated online service for the prediction of ADMET properties [105]. This service implements predictive QSAR models based on accurate and representative training sets, fragmental descriptors, and artificial neural networks. The quantitative estimate of drug-likeness (QED) values [106] were calculated using RDKit version 2021.09.2 software [107].

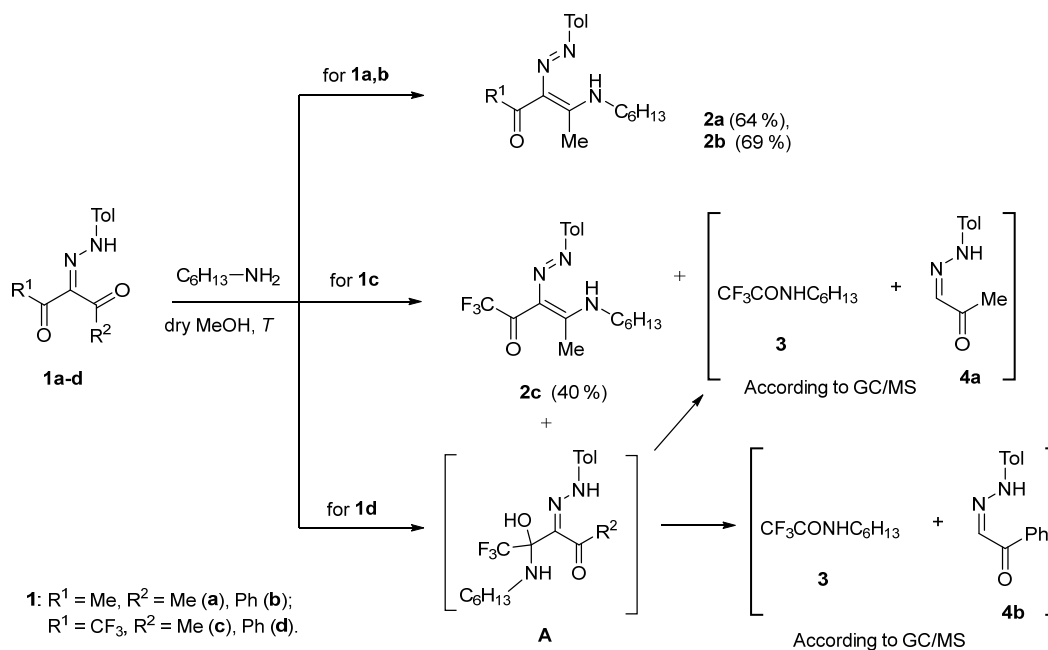
3. Results and Discussion

3.1. Chemistry

First, the interaction of 2-tolylhydrazinylidene-1,3-diketones **1a–d** with hexylamine was studied as a model reaction for the synthesis of conjugates with aminomethylene-modified tacrine. It was found that 2-tolylhydrazinylidene-substituted acetyl- and benzoylacetones **1a,b** reacted with hexylamine at the acetyl moiety in refluxing methanol to give products **2a,b** in good yields (Scheme 1). Note that the reaction of the benzoylacetone derivative **1b** bearing non-equivalent carbonyl centers proceeded chemoselectively to produce the only product **2b**. The regioisomeric structure of compound **2b** was established by ¹³C NMR spectroscopy. The signal of the carbonyl carbon atom in the ¹³C NMR spectrum was observed at δ 193 ppm, typical of the benzoyl fragment. The resonating signal of the acetyl group carbon atom in product **2a** was observed in the downfield region at δ 198 ppm [108].

The reaction of 1,1,1-trifluoro-3-[2-(4-methylphenyl)hydrazinylidene]pentane-2,4-dione **1c** and hexylamine occurred less selectively. This was confirmed by the formation of a mixture of products from which 1,1,1-trifluoro-4-hexylimine-3-(2-[4-methylphenyl]hydrazinylidene)pentan-2-one **2c** was isolated in moderate yield (Scheme 1). Its regioisomeric structure was confirmed by ¹³C NMR spectroscopy. In the ¹³C NMR spectrum of **2c**, the signal of the carbonyl atom at the CF₃ group was observed as a quartet in the same region at δ ~ 177 ppm as for the initial diketone **1c** [109]. We have shown earlier the preference in the condensation of trifluoromethyl-containing 2-arylhydrazinylidene-1,3-diketones at the carbonyl group of the non-fluorinated substituent for reactions with

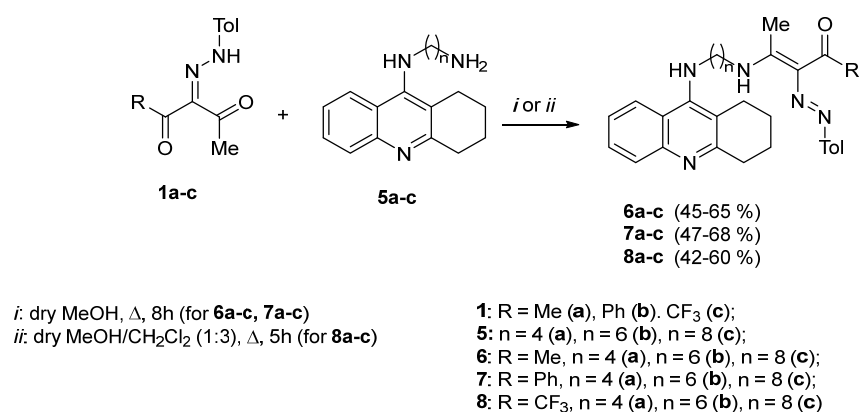
methylamine [110]. However, the mass spectrum of the reaction mixture had molecular ion peaks of 2,2,2-trifluoro-N-hexylacetamide **3** (m/z $[C_8H_{14}F_3NO]^+ = 198$) and 1-[2-(4-methylphenyl)hydrazinylidene]propan-2-one **4a** (m/z $[C_{10}H_{12}N_2O]^+ = 176$), formed as a result of competitive condensation of hexylamine at the carbonyl group with CF_3 substituent and subsequent cleavage of intermediate **A**. This side reaction resulted in a moderate yield of product **2c**.



Scheme 1. The reactions of 2-arylhidrazinylidene-1,3-diketones **1a-d** with hexylamine.

In contrast, the reaction of the 4,4,4-trifluoro-2-[2-(4-methylphenyl)hydrazinylidene]-1-phenylbutane-1,3-dione **1d** with hexylamine in refluxing methanol or at room temperature led to a mixture of products. According to the GC/MS, there were predominant peaks corresponding to molecular ions of 2,2,2-trifluoro-N-hexylacetamide **3** and 2-[2-(4-methylphenyl)hydrazinylidene]-1-phenylethan-1-one **4b** (m/z $[C_{15}H_{14}N_2O]^+ = 239$). In this case, the addition of hexylamine at the trifluoroacyl group of 1,3-diketone **1d** to form intermediate **A** and its subsequent cleavage to amide **3** and ketone **4b** were apparently to become preferable (Scheme 1). It should be noted that at room temperature incomplete conversion of the initial diketone **1d** along with the formation of cleavage products **3** and **4b** was observed, and at a temperature of 0–5 °C there were no noticeable changes in the initial reagents.

Then, it was found that 4-tolylhydrazinylidene-1,3-diketones **1a-c** react with aminomethylene tacrine derivatives **5a-c** (synthesized according to the methodology [81]) to give conjugates **6a-c**, **7a-c**, **8a-c** with various substituents in the diketone moiety and the length of the methylene linker (Scheme 2). The best yields of products **6a-c** and **7a-c** were achieved in the reactions of non-fluorinated 1,3-diketones **1a** and **1b** in dry methanol under reflux for 8 h. The reaction of the trifluoromethyl-containing analogue **1c** was carried out in a mixture of dry methylene chloride and dry methanol (3: 1) under reflux for 5 h. Note that the reaction in dry methanol or ethanol even at room temperature led to acidic cleavage of the starting 2-tolylhydrazinylidene-1,3-diketone **1c** and significantly reduced the yields of the target conjugates **8a-c**.

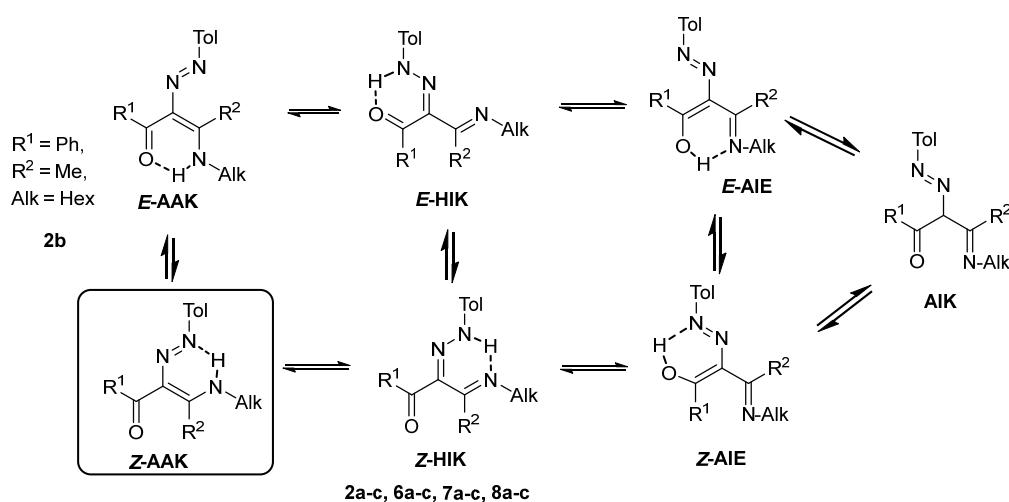


Scheme 2. Synthesis of conjugates **6**, **7**, **8**.

The regioisomeric structure of compounds **6a-c**, **7a-c**, **8a-c** was established by ¹³C NMR spectroscopy. In the spectra of acetylacetone derivatives **6a-c**, a characteristic signal of the carbonyl carbon atom of the acetyl group was observed at δ 198 ppm. In the case of benzoylacetone derivatives **7a-c**, the carbonyl carbon atom of the benzoyl fragment resonated at δ 193 ppm, while the spectra of trifluoroacetylacetone derivatives **8a-c** were characterized by a quartet signal of the trifluoroacetyl carbon atom at δ 177 ppm. It can be concluded that all compounds **6a-c**, **7a-c**, **8a-c** were formed by condensation of 1,3-diketones **1a-c** with tacrines **5a-c** at the acetyl fragment similarly to the reactions with hexylamine.

It should be noted that the reaction of diketone **1d** with tacrines **5a-c** was not effective despite attempts to vary the conditions.

The synthesized compounds **2a-c**, **6a-c**, **7a-c**, and **8a-c** have a hydrazone-diketone fragment with a mobile hydrogen atom. They can be characterized by prototropic imino-amine, azo-hydrazone and keto-enol tautomerism with the existence of four tautomeric forms **AAK**, **HIK**, **AIE**, and **AIK**, including *Z,E*-isomers for the first three forms (Scheme 3). All tautomers except **AIK** are stabilized by an intramolecular H-bond.



Scheme 3. Isomerism of compounds **2a-c**, **6a-c**, **7a-c**, and **8a-c**.

The ¹H NMR spectra of compounds **2a-c**, **6a-c**, **7a-c**, and **8a-c** in CDCl₃ did not contain the CH proton signal of the **AIK** form. Instead, a low-field signal of the proton of the HN- or HO-group was observed at δ 14.7–15.4 ppm and, as already mentioned, all ¹³C NMR spectra contained low-field signals of carbonyl carbon atoms. These spectral data allowed us to exclude the **AIK** and **AIE** tautomers from consideration.

The choice between tautomers **AAK** and **HIK** was made using ¹H NMR spectral data and our previous experience. We have earlier shown that 4-(*N*-methyl)amino-1,1,1-

trifluoro-3-phenylazopent-3-en-2-one [110] exists in the solid state as an *Z*-azo-amino-ketone tautomer (*Z*-AAK) according to X-ray diffraction data, and upon dissolution in chloroform transforms into the *Z*-hydrazo-keto-imine tautomer (*Z*-HIK), given that in its ^1H NMR spectrum the signal of the *N*-methyl group was observed as a singlet at δ 2.92 ppm. In contrast, in the ^1H NMR spectra of compounds **2a-c**, **6a-c**, **7a-c**, and **8a-c**, the signals of the N-CH_2 groups were observed as a triplet of doublets at δ 3.4–3.5 ppm due to interaction with the neighboring NH proton.

The ^1H and ^{13}C NMR spectra of products **2a,c**, **6a-c**, **7a-c**, **8a-c** in CDCl_3 contained one set of signals. The spectra of compound **2b** containing benzoyl and *N*-hexylamine substituents were characterized by the presence of a second set of signals, and its ^1H NMR spectrum exhibited two triplets of doublets of a HN-CH_2 group at δ 3.18 and 3.52 ppm, apparently due to the existence of compounds **2b** in the form of *Z,E*-isomers in a ratio of 87:13.

Based on the analysis performed, we believe that in a CDCl_3 solution, compounds **2a-c**, **6a-c**, **7a-c**, and **8a-c** predominantly exist in the *Z*-AAK form in contrast to the *N*-methyl analog [110] (Scheme 3).

We obtained monocrystals for compound **8a** by slow crystallization from acetonitrile. The XRD analysis showed that conjugate **8a** exists in the solid state also as *Z*-AAK (Figure 1) with formation of the intramolecular hydrogen bond between hydrogen H3 of NH group and nitrogen N2 of arylazo moiety (the distance $\text{H3}\cdots\text{N2}$ is 1.650 Å) similarly to the *N*-methyl analog [110]. The molecule of compound **8a** has an almost flat structure because 4-amino-1,1,1-trifluoro-3-(tolylidiazonyl)pent-3-en-2-one moiety and tacrine core are located in one plane. However, the butyl spacer C18C17C16C15 is characterized by distortions with 1.293 Å (for C18) and 1.131 Å (for C15) deviations from the common plane. The distance between nitrogens $\text{N3}\cdots\text{N4}$ connected with butyl linker is 5.304 Å.

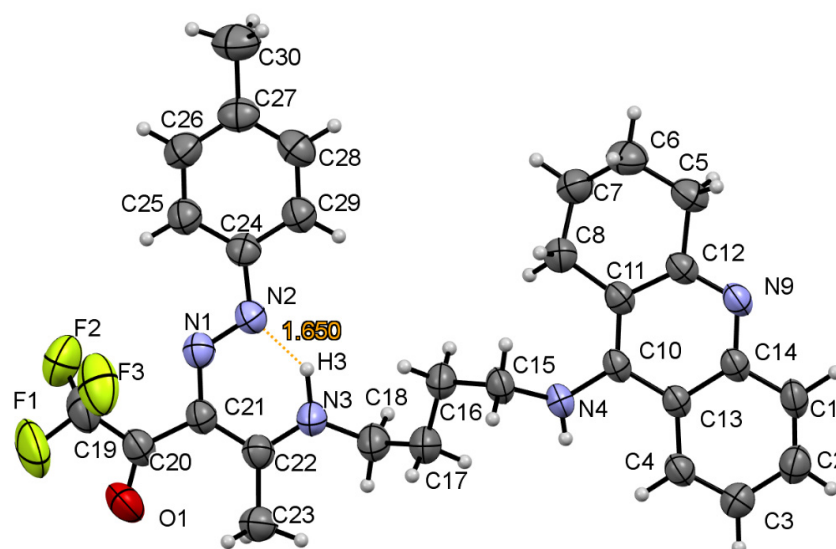


Figure 1. The ORTEP view of conjugate **8a**.

To assess computationally the relative stability of tautomers and conformers of the compounds **2a-c**, **6a-c**, **7a-c**, and **8a-c**, instead of manual generation of configurations of interest, as we have formerly done [79,87,111], we resorted to formal generation of tautomers with ChemAxon MarvinSketch. Next, geometries of all generated tautomers (from 34 for compounds **2b** and **2c** to 86 for compounds **6a-c**), were optimized quantum-mechanically. The optimized structures of the tautomers were subjected to conformational search with TorsiFlex. Because the conformational search led to a significant decrease of energy of certain tautomers (>20 kcal/mol for example of compound **8a**), it proved to be necessary to include in the conformational search all of the generated tautomers, instead of selecting some of them (e.g., top-10, or within 10 kcal/mol from the top tautomer).

The most stable conformation for compound **8a** found by TorsiFlex was of the *E*-AAK isomer. Chemically, *E/Z* isomerization of the double bond transforms it into a *Z*-AAK isomer. However, in terms of the conformational search, it is rotation around bond C21-C22 (according to Figure 1 labeling), that transforms the *E*-AAK isomer into *Z*-AAK. Multiple increases in the number of cycles of the conformational search led to the same *E*-AAK leading conformation, while the *Z*-AAK conformation was not found among the solutions. However, the presence in the results of other conformations requiring rotation around this bond but much higher in energy, proves that this torsion was included in the conformational search.

A manual flip around bond C21-C22 of the best conformational search solution transforming *E*-AAK into *Z*-AAK, followed by QM energy minimization, led to a 2.12 kcal/mol energy decrease, which is in agreement with the crystallographic results. Thus, formal generation of all possible tautomers followed by a conformational search required considerable computational resources but did not lead to the most stable configuration, while manual generation of possible isomers, tautomers, and major conformers proved to be more efficient.

The *Z*-AAK tautomer can be also transformed into *Z*-HIK via short-distance proton transfer. The energy profile of this process in vacuo was calculated for compound **8a** (Figure 2), yielding a 4.5 kcal/mol energy barrier and a 1.05 kcal/mol energy loss. Thus, the system predominantly exists in the *Z*-AAK form.

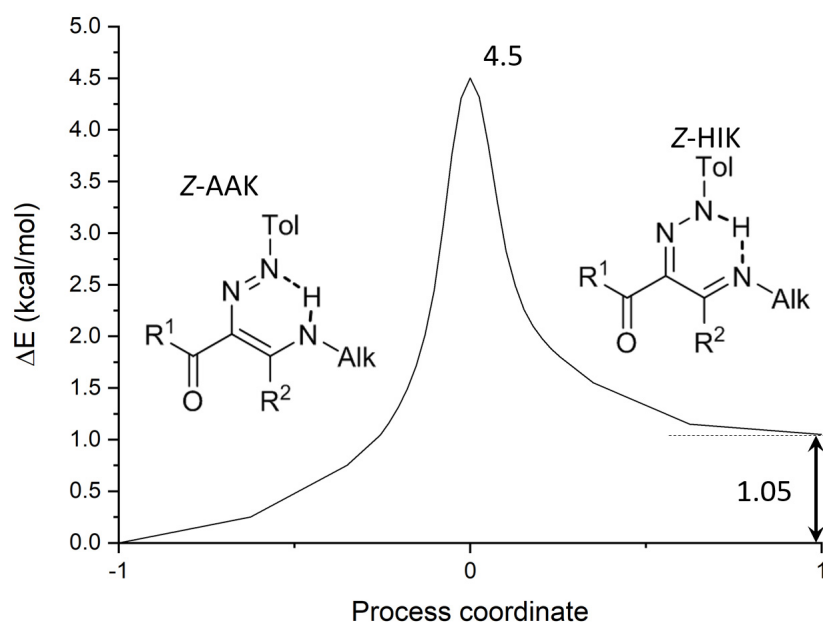


Figure 2. Energy profile of proton transfer between N2 and N3 atoms (according to Figure 1 labeling), transforming *Z*-AAK into the *Z*-HIK tautomer of compound **8a** ($R^1 = CF_3$, $R^2 = Me$).

3.2. Biological Studies

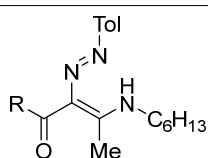
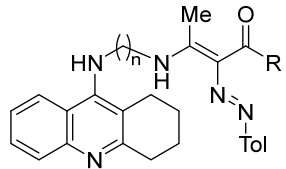
3.2.1. Esterase Profile Assessment

The method for evaluation of the esterase profile developed by our group includes the determination of the inhibitory activity of the synthesized compounds against enzymes of the cholinesterase family—AChE and BChE—as well as a structurally close enzyme—carboxylesterase (CES). Inhibition of AChE and BChE in the brain increases acetylcholine levels and improves cognitive functions in AD. CES is responsible for hydrolysis of numerous therapeutically important ester-containing drugs, and therefore inhibition of CES by anticholinesterase compounds used in AD therapy could lead to adverse drug-drug interactions.

Human erythrocyte AChE, equine serum BChE, and porcine liver CES were used to assess the esterase profile. The applicability of this set of enzymes for this purpose has

been shown earlier [112–115]. The results on the esterase profile of model compounds **2** and conjugates **6–8** are displayed in Table 1.

Table 1. Esterase profile of compounds **2**, **6**, **7**, **8** and their ability to displace propidium iodide from the peripheral anionic site of *Electrophorus electricus* AChE (*EeAChE*).

No	Compound Structure	Inhibitory Activity against AChE, BChE and CES			% Displacement of Propidium from the <i>EeAChE</i> PAS at 20 μ M
		IC ₅₀ , μ M or % Inhibition at 20 μ M			
		AChE	BChE	CES	
					
2a	R = Me	22.9 \pm 1.2%	18.1 \pm 0.8	n.a.	n.a.
2b	R = Ph	12.5 \pm 0.6%	25.0 \pm 2.0%	n.a.	n.a.
2c	R = CF ₃	14.7 \pm 3.2%	35.3 \pm 2.7%	n.a.	n.a.
					
	R = Me				
6a	n = 4	1.39 \pm 0.04	0.139 \pm 0.017	23.3 \pm 0.4%	15.6 \pm 1.2
6b	n = 6	0.342 \pm 0.015	0.138 \pm 0.002	29.0 \pm 0.1%	19.0 \pm 1.3
6c	n = 8	0.272 \pm 0.017	0.0543 \pm 0.0037	30.1 \pm 1.2%	17.8 \pm 1.4
	R = Ph				
7a	n = 4	0.889 \pm 0.007	0.0359 \pm 0.0020	31.2 \pm 2.9%	11.9 \pm 0.8
7b	n = 6	0.380 \pm 0.003	0.0470 \pm 0.0038	33.2 \pm 1.7%	15.5 \pm 1.3
7c	n = 8	0.249 \pm 0.020	0.0745 \pm 0.0060	23.4 \pm 2.2%	14.1 \pm 1.1
	R = CF₃				
8a	n = 4	1.69 \pm 0.05	0.246 \pm 0.016	28.6 \pm 4.0%	13.7 \pm 1.2
8b	n = 6	0.276 \pm 0.020	0.125 \pm 0.006	19.9 \pm 2.9%	14.4 \pm 1.3
8c	n = 8	0.241 \pm 0.014	0.0985 \pm 0.0013	12.2 \pm 1.7%	16.2 \pm 1.4
	Tacrine	0.601 \pm 0.047	0.0295 \pm 0.0002	n.a.	4.4 \pm 0.6
	Donepezil	0.0400 \pm 0.0037	19.2 \pm 2.0	n.a.	11.9 \pm 0.9
	BNPP	n.a.	n.a.	1.8 \pm 0.1	n.d.

Data are presented as mean \pm SEM, n = 3; n.a.—not active; n.d.—not determined.

The results presented in Table 1 indicate that compounds **2a–c**—*N*-hexylamine derivatives of 2-tolylhydrazinylidene-1,3-diketones **1a–c** inhibit cholinesterases very weakly and do not inhibit CES. At the same time, all 3 groups of conjugates of 2-tolylhydrazinylidene-1,3-diketones **1a–c** with tacrine **6**, **7**, and **8** exhibit high inhibitory activity against cholinesterases—at the level and above the parent pharmacophore tacrine with predominant inhibition of BChE and weak inhibition of CES.

Prior to the research, we feared that the synthesized conjugates **6**, **7**, and **8** might exhibit anti-CES activity undesirable for AD therapy agents, because we have previously found that one of the starting compounds, 2-tolylhydrazinylidene-1,3-diketone **1c**, exhibits moderate inhibitory activity against this enzyme [79]. However, it turned out that the isomerization of the hydrazone tautomer to the azo form upon replacement of one of the carbonyl groups by the alkylamine functional group led to a significant decrease in the anti-CES activity.

AChE inhibition. The structure of the R substituent at the carbonyl carbon atom (Me, Ph, or CF₃) had practically no effect on the anti-AChE activity of conjugates. At the same time, for all series of conjugates **6**, **7**, and **8**, an increase in inhibitory activity against AChE was observed with an increase in the spacer length (from 4 to 8 CH₂ groups). The anti-AChE activity of conjugates **6b,c**, **7b,c**, and **8b,c** was higher than the activity of the parent pharmacophore tacrine. Compounds **6c**, **7c**, **8b**, and **8c** exhibited the highest anti-AChE activity (IC₅₀ = 0.27, 0.25, 0.28 and 0.24 μM, respectively).

BChE inhibition. All conjugates were active against BChE. There was no pronounced effect of the spacer length on the inhibitory activity. However, anti-BChE activity depended on the structure of the R substituent at the carbonyl carbon atom: conjugates **7** with R = Ph were most active and reached the level of tacrine. The most effective BChE inhibitors were compounds **6c**, **7a**, **7b**, **7c** (IC₅₀ = 0.054, 0.036, 0.047, and 0.0745 μM, respectively).

The selectivity toward BChE compared to AChE is maximum for compounds with a short spacer (CH₂)₄; it is especially pronounced for **7a** (R = Ph).

3.2.2. Kinetic Studies of AChE and BChE Inhibition

The mechanism of inhibitory action of the conjugates toward AChE and BChE was studied using compound **6b** as a sample. The graphical analysis of the kinetic data on AChE (Figure 3A) and BChE (Figure 3B) inhibition by **6b** in the Lineweaver–Burk double-reciprocal plot demonstrates the changes in both K_m and V_{max} that attest to a mixed type of inhibition. The inhibition constants are as follows: $K_i = 0.254 \pm 0.018$ μM (competitive component) and $\alpha K_i = 0.473 \pm 0.041$ μM (noncompetitive component) for AChE and $K_i = 0.095 \pm 0.008$ μM (competitive component) and $\alpha K_i = 0.224 \pm 0.022$ μM (noncompetitive component) for BChE.

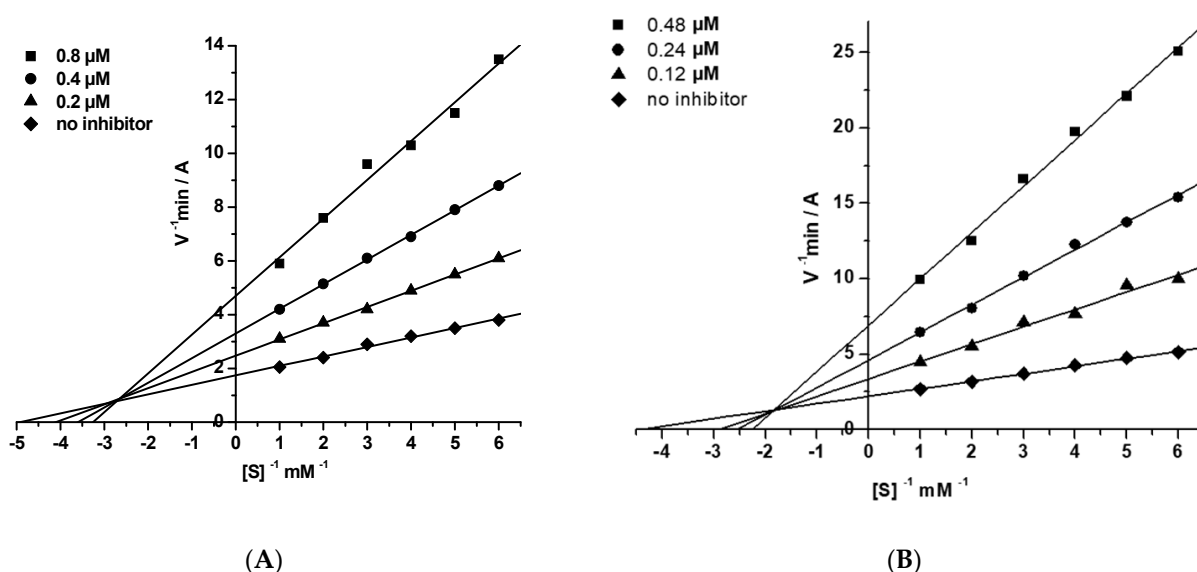


Figure 3. Steady state inhibition of (A) AChE and (B) BChE by compound **6b**. Lineweaver–Burk double-reciprocal plots of initial velocity and substrate concentrations in the presence of inhibitor (three concentrations) and without inhibitor are presented. The changes in both K_m and V_{max} attest to a mixed type of inhibition.

3.2.3. Molecular Modeling Studies

The most stable **Z-AAK** conformer of the considered compounds was taken for molecular docking studies. It was found that all compounds bind to the hAChE in a uniform way, occupying both the CAS and PAS. In the CAS, the protonated tacrine fragment binds forming π - π stacking interactions with the Trp86 side chain and a hydrogen bond with its main chain hydrogen oxygen (Figure 4A–C), as was observed previously for tacrine-containing conjugates [116,117]. Compounds **6a–c** also form a few hydrogen bonds between Tyr124

phenolic hydroxyl group and the linker nitrogen atoms or carbonyl atom of the acetyl group (Figure 4A). With increasing linker length, the tolyl substituent occupies more of the PAS, forming π - π or T-stacking interactions with Trp286. For compounds 7a–c these interactions are with the phenyl group, which is advancing into the PAS and interacting with Trp286, instead of with the tolyl substituent, while the latter protrudes out of the gorge entrance. Additionally, the carbonyl oxygen atom of the keto-group forms hydrogen bonds with the Phe295 and Arg296 main chain nitrogen atoms (Figure 4B).

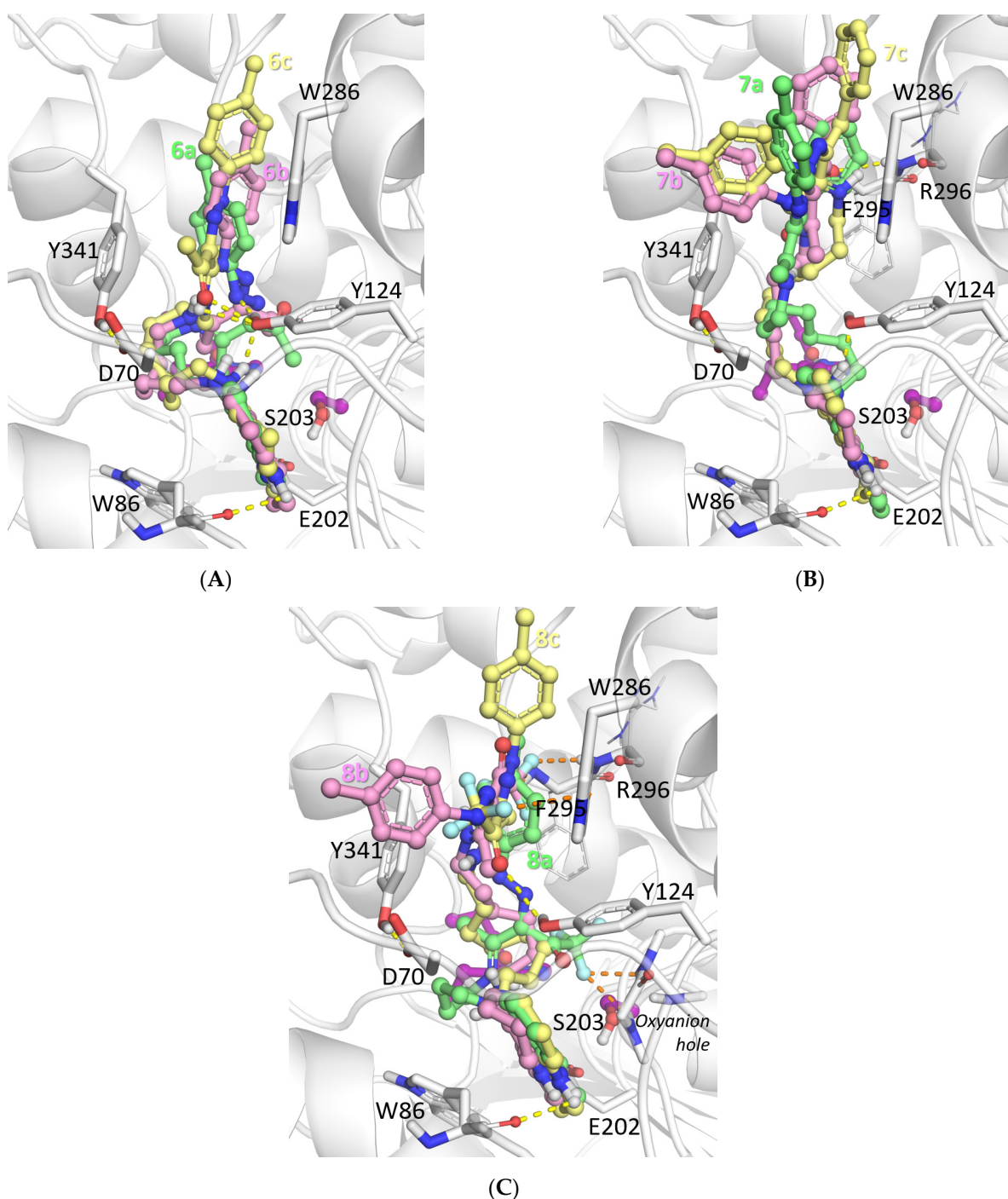


Figure 4. Molecular docking to the active site of AChE of conjugates 6a–c (A), 7a–c (B), and 8a–c (C). Carbon atoms of compounds 6–8a are colored green, 6–8b—pink, 6–8c—yellow.

Regarding compounds **8a-c** with a trifluoromethylketone (TFK) group, specific interactions change with elongation of the linker. For compound **8a**, one of the fluorine atoms was found in the oxyanion hole. For compound **8b**, it forms hydrogen bonds with the Phe295 and Arg296 main chain nitrogen atoms. For compound **8c**, it interacts with Trp286 side chain, forming an F- π contact [118] (Figure 4C). Such modes of interactions were previously observed for a TFK compound, sliding down the gorge [119]. However, in the present case, no position with the carbonyl oxygen atom in the oxyanion site was found, which excludes the possibility of a subsequent covalent reaction between the enzyme and inhibitor.

For all the groups of inhibitors, increasing occupancy of the PAS with elongation of the linker can be associated with an increase in the propidium displacement ability.

In the case of BChE, binding is much more uniform with the carbonyl oxygen atom of the keto group in the oxyanion hole (Figure 5A–C). While ligands with increasing linker length occupy similar positions in the BChE active site, the tacrine fragment could form π -cation and π - π stacking interactions with Tyr332 or Trp82, supported by ionic interactions and hydrogen bonds with the Asp70 or His438 main chain oxygen atom, respectively. In the case of compounds **7a-c**, there are additional π - π or T-stacking interactions of the tolyl substituent with the Trp231 side chain (Figure 5B). In the case of compounds **8a-c**, the trifluoromethyl group forms F- π interactions with the Trp231 side chain (Figure 5C). Overall, the position of the TFK group of compounds **8a-c** in the catalytic site of BChE suggests the subsequent formation of a labile covalent bond and an adduct, called a tetrahedral intermediate analog [119].

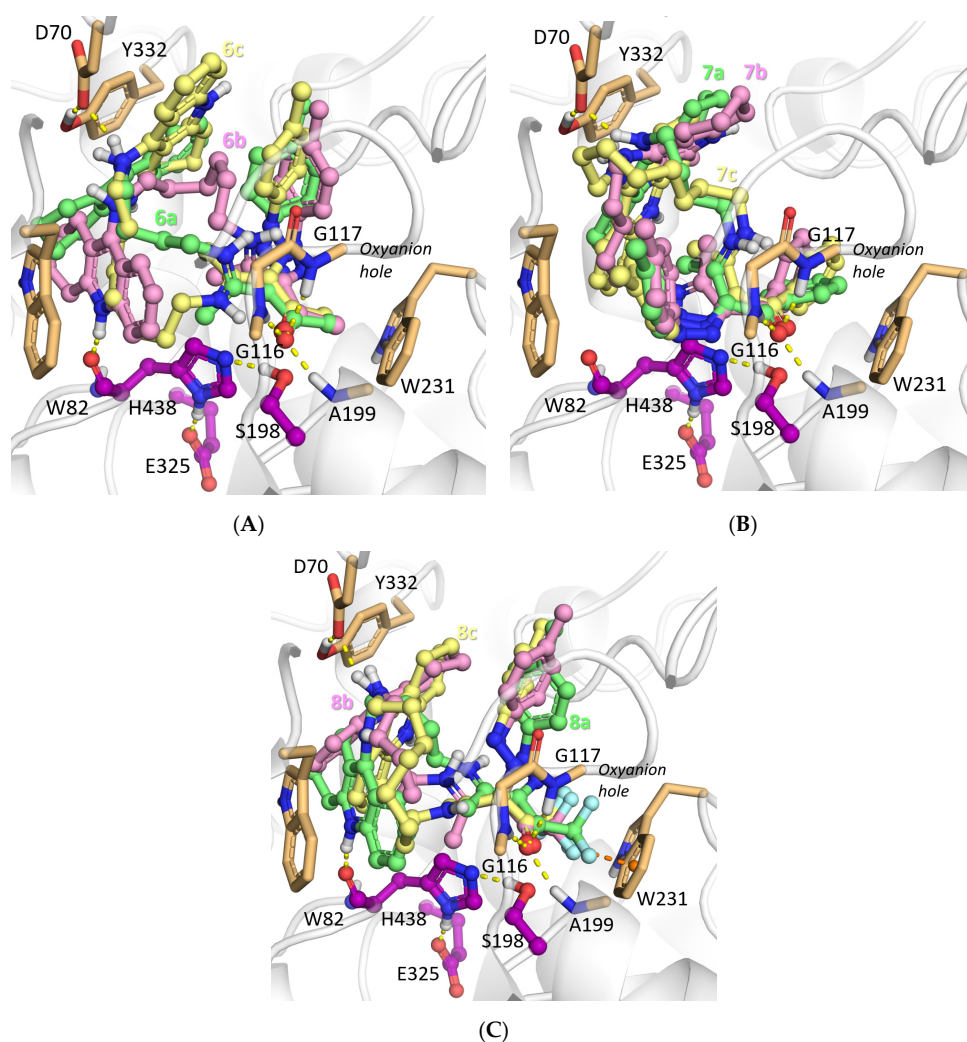


Figure 5. Molecular docking to the active site of BChE of conjugates **6a-c** (A), **7a-c** (B), and **8a-c** (C). Carbon atoms of compounds **6–8a** are colored green, **6–8b**—pink, **6–8c**—yellow.

3.2.4. Displacement of Propidium from the *EeAChE* PAS

The study of compounds as potential inhibitors of the proaggregant activity of AChE was carried out by assessment of the degree of displacement of the selective PAS ligand propidium iodide from the *EeAChE* PAS. As mentioned above, AChE PAS interacts with soluble A β peptides, promoting their aggregation. In this regard, compounds blocking the AChE PAS are potential antiaggregant agents.

As seen from Table 1, conjugates of tacrine with 2-tolylhydrazinylidene-1,3-diketones at a concentration of 20 μ M reduce the fluorescence intensity of the propidium iodide bound to *EeAChE* and displace propidium at or above the level of the control compound donepezil (11–19%). These data indicate the potential ability of conjugates to block AChE-induced aggregation of β -amyloid, which agrees with the mixed type inhibition of AChE by the conjugates (Figure 3A) and the results of molecular docking (Figure 4A–C). On the whole, the ability to displace propidium in all groups of conjugates 6, 7, and 8 increases with spacer elongation in agreement with the molecular docking results. The conjugates 6a–c (R = Me) exhibit the highest activity, displacing propidium from *EeAChE* PAS in the range of 15.6–19%, while the optimal spacer length is n = 6.

3.2.5. Antioxidant Activity

We have earlier shown [79] that 2-arylhydrazylidene-1,3-diketones 1c,d exhibit high radical-scavenging activity in the ABTS assay. Herein, we studied the primary antioxidant activity of a series of model compounds—aminoenketones 2a–c, and conjugates 6a–c, 7a–c, 8a–c, obtained from diketone 1c and its non-fluorinated analogs 1a,b.

The antioxidant activity of the compounds 2a–c, 6a–c, 7a–c, 8a–c was assessed by spectrophotometric ABTS and FRAP tests. The ABTS assay evaluates the binding of a model ABTS radical cation (ABTS \bullet^+), which is realized by the mechanism of single electron transfer (SET) and/or hydrogen atom transfer (HAT). The FRAP assay (Ferric Reducing Antioxidant Power) measures the ability of compounds to reduce the ferric 2,4,6-tripyridyl-s-triazine complex [Fe(TPTZ) $_2$] $^{3+}$ to [Fe(TPTZ) $_2$] $^{2+}$, which occurs exclusively by the SET mechanism. The results are presented in Table 2.

It was found that model compounds aminoenketones 2a–c, which are the reaction products of the interaction of 2-arylhydrazinylidene-1,3-diketones 1a–c (Scheme 1) with hexylamine, exhibit high radical-scavenging activity in the ABTS assay at the level of the standard antioxidant Trolox. The activity of the compounds did not depend on the substituent R at the carbonyl carbon atom (CH $_3$, Ph or CF $_3$). Conjugates 6a–c, 7a–c, 8a–c, which are a combination of 2-arylhydrazinylidene-1,3-diketones 1a–c and the anticholinesterase pharmacophore tacrine retained high ABTS \bullet^+ -scavenging activity of diketones at the Trolox level. The variation of the substituent R at the carbonyl carbon atom, as well as the spacer length, practically did not affect the radical-scavenging activity of the conjugates.

In the FRAP assay, the model compounds 2a,b and conjugates 6a–c, 7a–c, also demonstrated fairly good activity. However, their activity in the FRAP test was twice lower than in the ABTS test.

The most notable finding was that there was no influence of the structure of the R group in the carbonyl fragment on the activity in the ABTS test: both aminoenketone 2 and conjugates of 1,3-diketones with tacrine 6–8 were highly active. At the same time, in the FRAP test, compound 2c with R=CF $_3$ was not active and a weak ferric reducing ability was observed for conjugates 8a–c with the CF $_3$ substituent in the carbonyl moiety. Taking into account that the FRAP assay measures the Fe $^{3+}$ reducing ability occurring exclusively by the SET mechanism, whereas the binding of the ABTS radical cation can be realized by SET and/or HAT mechanisms, the observed different structure-activity relationships (in particular, no decrease in activity in the ABTS test for compounds 8a–c with a CF $_3$ substituent) may indicate different mechanisms of the antioxidant action of the studied compounds in the ABTS and FRAP tests. That is, the SET mechanism may be involved in the ferric reducing test and the HAT may be operating in the scavenging of the ABTS radical cation.

Table 2. Antioxidant activity of compounds **2a–c**, **6a–c**, **7a–c**, **8a–c**.

No	Compound Structure	Antioxidant Activity (mean \pm SEM)		
		ABTS ^{•+} -Scavenging Activity (n=3, 1 h, t = 30 °C)		FRAP (Fe ³⁺ -Reducing Activity) (n=3, 1 h, t = 37 °C)
		TEAC *	IC ₅₀ **, μ M	TE *
2a	R = Me	0.94 \pm 0.03	20.3 \pm 1.6	0.57 \pm 0.02
2b	R = Ph	0.98 \pm 0.03	18.9 \pm 1.2	0.52 \pm 0.02
2c	R = CF ₃	1.00 \pm 0.04	19.9 \pm 1.4	n.a.
	R = Me			
6a	n = 4	1.00 \pm 0.03	19.5 \pm 1.1	0.37 \pm 0.06
6b	n = 6	1.00 \pm 0.02	18.6 \pm 1.4	0.48 \pm 0.04
6c	n = 8	0.80 \pm 0.03	27.5 \pm 1.6	0.49 \pm 0.05
	R = Ph			
7a	n = 4	0.90 \pm 0.04	22.3 \pm 1.9	0.43 \pm 0.04
7b	n = 6	0.91 \pm 0.03	21.8 \pm 1.6	0.51 \pm 0.06
7c	n = 8	0.92 \pm 0.03	21.8 \pm 1.6	0.58 \pm 0.03
	R = CF₃			
8a	n = 4	1.13 \pm 0.05	17.7 \pm 1.3	0.06 \pm 0.01
8b	n = 6	1.00 \pm 0.04	17.9 \pm 0.6	0.11 \pm 0.03
8c	n = 8	0.95 \pm 0.03	19.4 \pm 1.3	0.12 \pm 0.01
	Trolox	1.0	19.7 \pm 0.8 (n=8)	1.0
	Ascorbic acid	0.96 \pm 0.02	22.6 \pm 1.3 (n=8)	1.23 \pm 0.11

* TEAC—trolox equivalent antioxidant capacity (ABTS) and TE (FRAP—antioxidant activity in Trolox equivalents (for the calculation method, see Experimental). ** compound concentration required for 50% reduction in the concentration of ABTS radical cation.

3.2.6. Metal-chelating Properties

It is known that decreasing excess concentrations of metals in the brain by chelating agents is one of the approaches to AD treatment [51,52]. The complexation abilities of compounds **6a**, **7a**, **8a** for biometals such as Cu²⁺, Fe²⁺ and Zn²⁺ in acetonitrile were studied by UV–Vis spectrometry [81] and the results for conjugates **6a**, **7a**, **8a** are shown in Figure 6A–C. In the UV–Vis spectra of **6a**, **7a**, **8a**, very broad bands from 340 to 470 nm and from 280 to 340 nm are ascribed to π - π^* transitions, and the peak around 240 nm is due to intramolecular charge transfer.

The spectra of the individual ions and compounds were subtracted from the spectra of the mixtures of each compound with each ion. A red shift of absorbance calculated in this way indicates the formation of a ligand-ion complex in the mixture. For example (Figure 7), it can be seen that there are two red shifts of absorbance from 240 to 253 nm and from 328 to 339 nm for the interaction of conjugate **8a** with Zn²⁺. For additional graphics, please see Supplementary, Figures S1–S8. The results obtained demonstrate metal-chelating ability for conjugates **6a**, **7a**, and **8a** to all three biometal ions (Cu²⁺, Fe²⁺ and Zn²⁺).

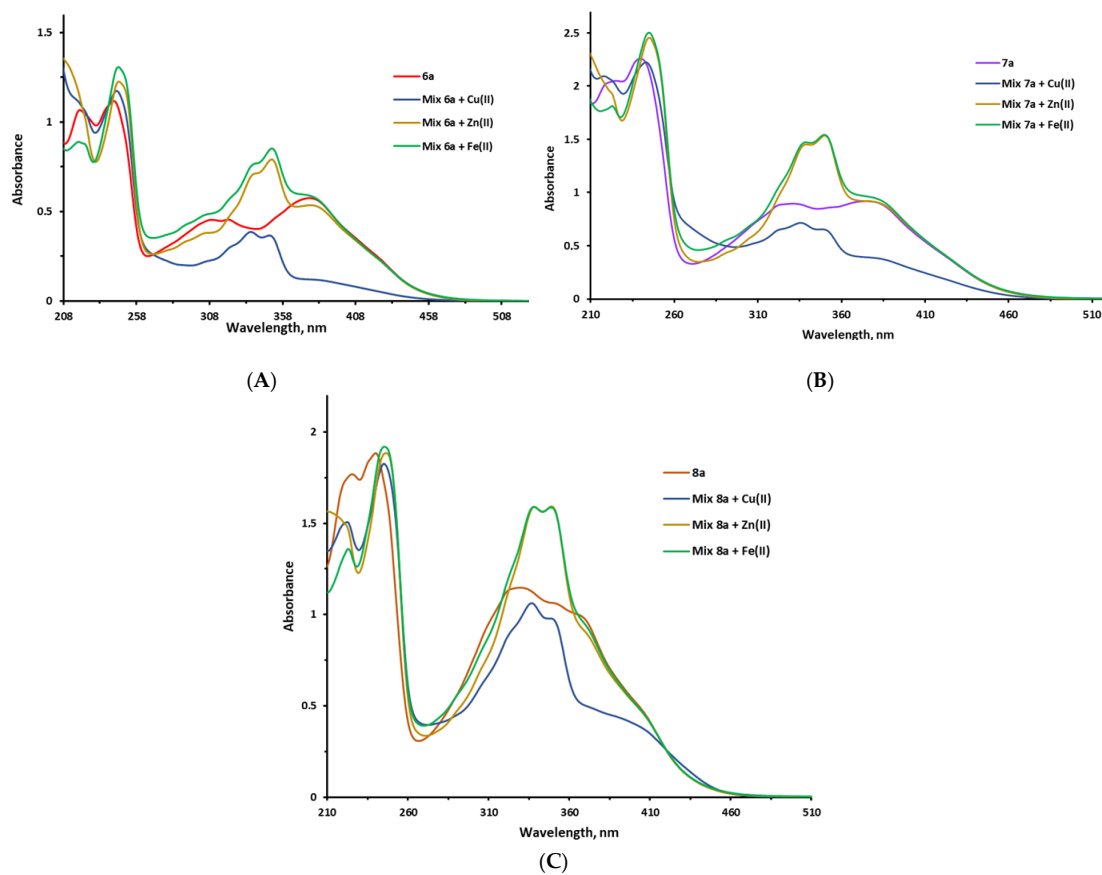


Figure 6. Absorption spectra of compounds **6a** (A), **7a** (B) and **8a** (C) in a concentration of 40 μM and their mixture with Cu^{2+} , Zn^{2+} , Fe^{2+} ions solution (40 μM) in acetonitrile solution at 25 $^{\circ}\text{C}$.

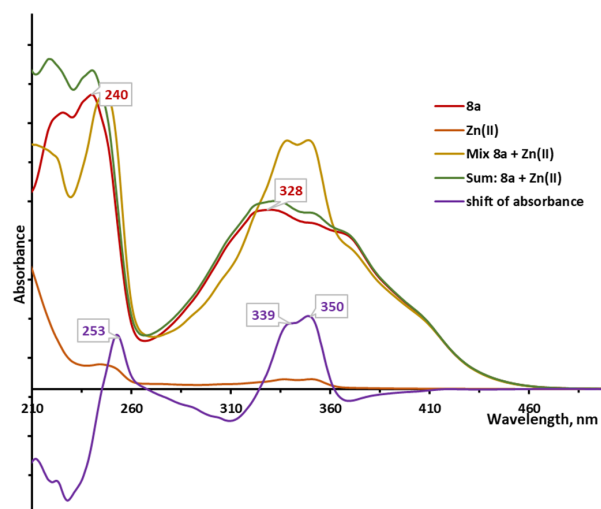


Figure 7. Absorption spectra of compound **8a** (40 μM), Zn^{2+} ion solution (40 μM), a sum of **8a** and Zn^{2+} , their mixture, and the shift of the spectra caused by the formation of a complex.

3.2.7. Prediction of ADMET and Physicochemical Profiles

The results of our computational estimates of selected ADMET and physicochemical properties for compounds **2**, **6–8** are shown in Table 3. All of the compounds had high predicted values for intestinal absorption, enabling their oral administration. Moreover, we could expect reasonable CNS activity in view of rather high predicted blood–brain barrier permeability (brain concentration exceeds the plasma concentration), although some

optimization of this parameter might be desirable. The cardiac toxicity risk parameters (hERG pK_i and pIC_{50}) fell within 4.2–7.6 log units for all the analyzed compounds, which was within the lower or medium part of their possible range (3–9 log units). According to the commonly accepted drug-likeness guidelines, the predicted lipophilicities and aqueous solubilities, as well as the molecular weights of the compounds, were within or close to the desirable range for potential drug compounds, although the LogP values in some cases violated the original Rule-of-5 limits (however, given that some of the compounds were outside of the model applicability domain, the predicted values were not fully reliable). The integral quantitative estimates of drug-likeness (QED) were in the 0.1–0.4 range.

Table 3. Predicted ADMET and physicochemical profiles of compounds **2**, **6–8**.

Compound	MW	LogP _{ow}	pS _{aq}	LogBB	HIA, %	hERG pK_i	hERG pIC_{50}	QED
2a	301.43	4.77	5.41	0.50	100	4.22	5.38	0.39
2b	363.51	5.96	6.83	0.65	98	4.72	6.07	0.23
2c	355.41	5.31	6.44	0.63	88	4.22	5.56	0.36
6a	469.63	5.97	7.03	0.23	100	4.56	6.11	0.19
6b	497.69	6.47	7.60	0.22	100	4.39	6.43	0.15
6c	525.74	6.89	7.46	0.59	100	4.72	6.88	0.13
7a	531.70	6.53	7.45	0.38	100	5.06	6.78	0.09
7b	559.76	6.93	7.69	0.38	100	4.88	7.12	0.07
7c	587.81	7.26	7.76	0.74	100	5.22	7.60	0.06
8a	523.60	6.28	7.40	0.36	93	4.56	6.27	0.17
8b	551.66	6.73	7.81	0.35	93	4.39	6.58	0.14
8c	579.71	7.11	7.90	0.72	93	4.72	7.01	0.11
Tacrine	198.27	2.95	1.52	−0.00	93	4.98	4.98	0.71

MW—molecular weight, LogP_{ow}—octanol-water partition coefficient, pS_{aq}—aqueous solubility [−log(M)], LogBB—blood–brain barrier distribution, HIA—human intestinal absorption [%], hERG pK_i —hERG potassium channel affinity [−log(M)], hERG pIC_{50} —hERG potassium channel inhibitory activity [−log(M)], QED—quantitative estimate of drug-likeness.

Consequently, the predicted ADMET and physicochemical properties of the compounds were acceptable for potential lead compounds in the discovery phase. Nevertheless, additional studies and structure optimization would be desirable to help maximize safety and improve the pharmacokinetic profile.

4. Conclusions

In summary, we synthesized the new conjugates of tacrine modified with 2-tolylazo-1,3-aminoenketone moieties with various acyl substituents through alkylene spacers of different lengths. According to NMR spectroscopy, the compounds were characterized by a predominant existence in solutions as a (Z)-2-azo-1,3-aminoenketone tautomer. According to XRD, compound **8a** in crystals also exists in (Z)-2-azo-1,3-aminoenketone form that agrees with QM calculations.

In general, conjugates **6a-c**, **7a-c**, **8a-c** demonstrated high inhibitory activity against both cholinesterases AChE and BChE, with selectivity for BChE, being mixed type inhibitors of both cholinesterases, and with weak inhibition of CES.

The structure of the R substituent at the carbonyl carbon atom (Me, Ph, or CF₃) had practically no effect on the anti-AChE activity of the conjugates. However, an increase in inhibitory activity was observed for all conjugates upon elongation of the alkylene spacer, in agreement with the results of molecular docking. Thus, a considerable group of compounds **6b,c**, **7b,c**, **8b,c** showed high anti-AChE activity exceeding the activity of tacrine: IC₅₀ = 0.24–0.34 μM.

The synthesized conjugates demonstrated high inhibitory activity against BChE. Their binding in the BChE active site was more uniform than seen with AChE, with the carbonyl oxygen atom of the keto group in the oxyanion hole. The most active inhibitors of BChE were compounds **6c** and **7a-c** (IC₅₀ = 0.036–0.0745 μM), which reached the activity of tacrine.

All conjugates **6–8** showed a good ability to displace propidium from *Ee*AChE PAS that along with the mixed type of inhibition revealed by the kinetics study and the molecular docking results indicates their potential ability to block AChE-induced aggregation of Aβ.

The synthesized conjugates have good antioxidant potency. All compounds **6–8** demonstrated the ability to effectively scavenge ABTS radical cation at the Trolox level; compounds **6, 7** also showed rather high Fe^{3+} reducing activity in the FRAP test. Moreover, metal-chelating ability for biometals such as Cu^{2+} , Fe^{2+} and Zn^{2+} was demonstrated for conjugates **6a, 7a**, and **8a**.

Finally, computational predictions of physico-chemical and ADMET properties of the compounds were consistent with drug-like characteristics and low toxicity.

The obtained results allowed us to consider the synthesized conjugates as new multifunctional agents for the potential treatment of AD. In particular, the non-fluorinated conjugates **6b,c, 7b,c** with $(\text{CH}_2)_6$ and $(\text{CH}_2)_8$ linkers exhibited the most promising set of properties and are recommended for further in-depth studies, e.g., lipid peroxidation in brain homogenates, neuroprotective activity in cell cultures, cognition enhancing efficacy in animal models, and safety and bioavailability assessments.

Supplementary Materials: The following supporting information can be downloaded at: <https://www.mdpi.com/article/10.3390/biom12111551/s1>: Figure S1. Absorption spectra of compound **6a** (40 μM), Cu^{2+} ions solution (40 μM), a sum of **6a** and Cu^{2+} , their mixture, and the shift of the spectra caused by the formation of a complex; Figure S2. Absorption spectra of compound **6a** (40 μM), Zn^{2+} ions solution (40 μM), a sum of **6a** and Zn^{2+} , their mixture, and the shift of the spectra caused by the formation of a complex; Figure S3. Absorption spectra of compound **6a** (40 μM), Fe^{2+} ions solution (40 μM), a sum of **6a** and Fe^{2+} , their mixture, and the shift of the spectra caused by the formation of a complex; Figure S4. Absorption spectra of compound **7a** (40 μM), Cu^{2+} ions solution (40 μM), a sum of **7a** and Cu^{2+} , their mixture, and the shift of the spectra caused by the formation of a complex; Figure S5. Absorption spectra of compound **7a** (40 μM), Zn^{2+} ions solution (40 μM), a sum of **7a** and Zn^{2+} , their mixture, and the shift of the spectra caused by the formation of a complex; Figure S6. Absorption spectra of compound **7a** (40 μM), Fe^{2+} ions solution (40 μM), a sum of **7a** and Fe^{2+} , their mixture, and the shift of the spectra caused by the formation of a complex; Figure S7. Absorption spectra of compound **8a** (40 μM), Cu^{2+} ions solution (40 μM), a sum of **8a** and Cu^{2+} , their mixture, and the shift of the spectra caused by the formation of a complex; Figure S8. Absorption spectra of compound **8a** (40 μM), Fe^{2+} ions solution (40 μM), a sum of **8a** and Fe^{2+} , their mixture, and the shift of the spectra caused by the formation of a complex; Figure S9. IC_{50} values for AChE inhibition by compounds **6a, 7a, 8a** (MEAN \pm SEM, $n = 3$); Figure S10. IC_{50} values for BChE inhibition by compounds **6a, 7a, 8a** (mean \pm SEM, $n = 3$); Figure S11. IR spectrum of compound **2a**; Figure S12. ^1H NMR spectrum of compound **2a**; Figure S13. ^{13}C NMR spectrum of compound **2a**; Figure S14. IR spectrum of compound **2b**; Figure S15. ^1H NMR spectrum of compound **2b**; Figure S16. ^{13}C NMR spectrum of compound **2b**; Figure S17. IR spectrum of compound **2c**; Figure S18. ^1H NMR spectrum of compound **2c**; Figure S19. ^{13}C NMR spectrum of compound **2c**; Figure S20. ^{19}F NMR spectrum of compound **2c**; Figure S21. IR spectrum of compound **6a**; Figure S22. ^1H NMR spectrum of compound **6a**; Figure S23. ^{13}C NMR spectrum of compound **6a**; Figure S24. IR spectrum of compound **6b**; Figure S25. ^1H NMR spectrum of compound **6b**; Figure S26. ^{13}C NMR spectrum of compound **6b**; Figure S27. IR spectrum of compound **6c**; Figure S28. ^1H NMR spectrum of compound **6c**; Figure S29. ^{13}C NMR spectrum of compound **6c**; Figure S30. IR spectrum of compound **7a**; Figure S31. ^1H NMR spectrum of compound **7a**; Figure S32. ^{13}C NMR spectrum of compound **7a**; Figure S33. IR spectrum of compound **7b**; Figure S34. ^1H NMR spectrum of compound **7b**; Figure S35. ^{13}C NMR spectrum of compound **7b**; Figure S36. IR spectrum of compound **7c**; Figure S37. ^1H NMR spectrum of compound **7c**; Figure S38. ^{13}C NMR spectrum of compound **7c**; Figure S39. IR spectrum of compound **8a**; Figure S40. ^1H NMR spectrum of compound **8a**; Figure S41. ^{13}C NMR spectrum of compound **8a**; Figure S42. ^{19}F NMR spectrum of compound **8a**; Figure S43. IR spectrum of compound **8b**; Figure S44. ^1H NMR spectrum of compound **8b**; Figure S45. ^{13}C NMR spectrum of compound **8b**; Figure S46. ^{19}F NMR spectrum of compound **8b**; Figure S47. IR spectrum of compound **8c**; Figure S48. ^1H NMR spectrum of compound **8c**; Figure S49. ^{13}C NMR spectrum of compound **8c**; Figure S50. ^{19}F NMR spectrum of compound **8c**.

Author Contributions: Conceptualization, methodology, G.F.M., Y.V.B.; synthesis, N.A.E., M.V.G., E.V.S., A.N.P. and L.S.L.; experimental investigation, N.V.K., E.V.R. (Elena V. Rudakova), N.P.B. and E.F.Z.; computer modeling, S.V.L., T.Y.A., E.V.R. (Eugene V. Radchenko), V.A.P. and R.J.R.; writing—original draft preparation, E.V.S., N.V.K., E.V.R. (Elena V. Rudakova), N.P.B., E.F.Z., S.V.L. and E.V.R. (Eugene V. Radchenko); writing—review and editing, G.F.M., Y.V.B., E.V.S., V.I.S., S.V.L. and E.V.R. (Eugene V. Radchenko), V.A.P. and R.J.R.; supervision, G.F.M., R.J.R. and V.I.S. All authors have read and agreed to the published version of the manuscript.

Funding: This work was supported by the Russian Foundation for Basic Research (Project No. 20-33-90204) and by the Ministry of Science and Higher Education of the Russian Federation (Project No. AAAA-A19-119012490007-8). Molecular modelling and antioxidant activity assay were performed in the frame of RFBR Project No 20-03-00590 and IPAC RAS State Targets Project FFSN-2021-0005. Support for RJR’s contributions to the computer modeling components of the work was provided in part by a grant from the Alternatives Research & Development Foundation (ARDF) and an Mcubed grant from the University of Michigan. The funding sources had no role in the study design; collection, analysis and interpretation of data; writing of the manuscript; or the decision to submit the article for publication.

Institutional Review Board Statement: Not applicable.

Informed Consent Statement: Not applicable.

Data Availability Statement: Not applicable.

Acknowledgments: Analytical studies (IR, UV-vis and NMR spectroscopy, and XRD analysis experiments) were carried out using equipment of the Center for Joint Use “Spectroscopy and Analysis of Organic Compounds” at the Postovsky Institute of Organic Synthesis of UB RAS. We thank the shared research facilities of the HPC computing resources at Lomonosov Moscow State University [120] for supercomputer time and the “Centre for Collective Use of IPAC RAS” for using the equipment cited in the Methods.

Conflicts of Interest: The authors declare no conflict of interest.

References

- 2020 Alzheimer’s disease facts and figures. *Alzheimers. Dement.* **2020**, *16*, 391–460. [CrossRef]
- Gandy, S.; DeKosky, S.T. Toward the Treatment and Prevention of Alzheimer’s Disease: Rational Strategies and Recent Progress. *Annu. Rev. Med.* **2013**, *64*, 367–383. [CrossRef]
- Albertini, C.; Salerno, A.; de Sena Murteira Pinheiro, P.; Bolognesi, M.L. From combinations to multitarget-directed ligands: A continuum in Alzheimer’s disease polypharmacology. *Med. Res. Rev.* **2020**, *41*, 1–28. [CrossRef]
- Bartus, R.T. On Neurodegenerative Diseases, Models, and Treatment Strategies: Lessons Learned and Lessons Forgotten a Generation Following the Cholinergic Hypothesis. *Exp. Neurol.* **2000**, *163*, 495–529. [CrossRef]
- Bachurin, S.O. Medicinal chemistry approaches for the treatment and prevention of Alzheimer’s disease. *Med. Res. Rev.* **2003**, *23*, 48–88. [CrossRef]
- Allgaier, M. An update on drug treatment options of Alzheimer’s disease. *Front. Biosci.* **2014**, *19*, 1345–1354. [CrossRef]
- Martinez, A.; Castro, A. Novel cholinesterase inhibitors as future effective drugs for the treatment of Alzheimer’s disease. *Expert. Opin. Investig. Drugs* **2006**, *15*, 1–12. [CrossRef]
- Duysen, E.G.; Li, B.; Darvesh, S.; Lockridge, O. Sensitivity of butyrylcholinesterase knockout mice to (–)-huperzine A and donepezil suggests humans with butyrylcholinesterase deficiency may not tolerate these Alzheimer’s disease drugs and indicates butyrylcholinesterase function in neurotransmission. *Toxicology* **2007**, *233*, 60–69. [CrossRef]
- Giacobini, E. Cholinesterases: New Roles in Brain Function and in Alzheimer’s Disease. *Neurochem. Res.* **2003**, *28*, 515–522. [CrossRef]
- Giacobini, E. Cholinergic function and Alzheimer’s disease. *Int. J. Geriatr. Psychiatry* **2003**, *18*, S1–S5. [CrossRef]
- Greig, N.H.; Utsuki, T.; Ingram, D.K.; Wang, Y.; Pepeu, G.; Scali, C.; Yu, Q.-S.; Mamczarz, J.; Holloway, H.W.; Giordano, T.; et al. Selective butyrylcholinesterase inhibition elevates brain acetylcholine, augments learning and lowers Alzheimer -amyloid peptide in rodent. *Proc. Natl. Acad. Sci. USA* **2005**, *102*, 17213–17218. [CrossRef]
- Mesulam, M.-M.; Guillozet, A.; Shaw, P.; Levey, A.; Duysen, E.G.; Lockridge, O. Acetylcholinesterase knockouts establish central cholinergic pathways and can use butyrylcholinesterase to hydrolyze acetylcholine. *Neuroscience* **2002**, *110*, 627–639. [CrossRef]
- Ballard, C.; Greig, N.; Guillozet-Bongaarts, A.; Enz, A.; Darvesh, S. Cholinesterases: Roles in the Brain During Health and Disease. *Curr. Alzheimer Res.* **2005**, *2*, 307–318. [CrossRef]
- Furukawa-Hibi, Y.; Alkam, T.; Nitta, A.; Matsuyama, A.; Mizoguchi, H.; Suzuki, K.; Moussaoui, S.; Yu, Q.-S.; Greig, N.H.; Nagai, T.; et al. Butyrylcholinesterase inhibitors ameliorate cognitive dysfunction induced by amyloid- β peptide in mice. *Behav. Brain Res.* **2011**, *225*, 222–229. [CrossRef]

15. Lane, R.M.; Potkin, S.G.; Enz, A. Targeting acetylcholinesterase and butyrylcholinesterase in dementia. *Int. J. Neuropsychopharmacol.* **2005**, *9*, 101–124. [[CrossRef](#)]
16. Macdonald, I.R.; Rockwood, K.; Martin, E.; Darvesh, S. Cholinesterase Inhibition in Alzheimer's Disease: Is Specificity the Answer? *J. Alzheimers Dis.* **2014**, *42*, 379–384. [[CrossRef](#)]
17. Calabrò, M.; Rinaldi, C.; Santoro, G.; Crisafulli, C. The biological pathways of Alzheimer disease: A review. *AIMS Neurosci.* **2021**, *8*, 86–132. [[CrossRef](#)]
18. Long, J.M.; Holtzman, D.M. Alzheimer Disease: An Update on Pathobiology and Treatment Strategies. *Cell* **2019**, *179*, 312–339. [[CrossRef](#)]
19. Bachurin, S.O.; Bovina, E.V.; Ustyugov, A.A. Drugs in clinical trials for Alzheimer's disease: The major trends. *Med. Res. Rev.* **2017**, *37*, 1186–1225. [[CrossRef](#)]
20. Hardy, J.; Bogdanovic, N.; Winblad, B.; Portelius, E.; Andreasen, N.; Cedazo-Minguez, A.; Zetterberg, H. Pathways to Alzheimer's disease. *J. Intern. Med.* **2014**, *275*, 296–303. [[CrossRef](#)]
21. Hsiao, K.; Chapman, P.; Nilsen, S.; Eckman, C.; Harigaya, Y.; Younkin, S.; Yang, F.; Cole, G. Correlative Memory Deficits, A Elevation, and Amyloid Plaques in Transgenic Mice. *Science* **1996**, *274*, 99–103. [[CrossRef](#)]
22. De Ferrari, G.V.; Canales, M.A.; Shin, I.; Weiner, L.M.; Silman, I.; Inestrosa, N.C. A Structural Motif of Acetylcholinesterase That Promotes Amyloid β -Peptide Fibril Formation †. *Biochemistry* **2001**, *40*, 10447–10457. [[CrossRef](#)]
23. Inestrosa, N.C.; Dinamarca, M.C.; Alvarez, A. Amyloid-cholinesterase interactions. *FEBS Journal* **2008**, *275*, 625–632. [[CrossRef](#)]
24. Arce, M.P.; Rodríguez-Franco, M.I.; González-Muñoz, G.C.; Pérez, C.; López, B.; Villarroja, M.; López, M.G.; García, A.G.; Conde, S. Neuroprotective and Cholinergic Properties of Multifunctional Glutamic Acid Derivatives for the Treatment of Alzheimer's Disease. *J. Med. Chem.* **2009**, *52*, 7249–7257. [[CrossRef](#)]
25. Rouleau, J.; Iorga, B.I.; Guillou, C. New potent human acetylcholinesterase inhibitors in the tetracyclic triterpene series with inhibitory potency on amyloid β aggregation. *Eur. J. Med. Chem.* **2011**, *46*, 2193–2205. [[CrossRef](#)]
26. Darvesh, S.; Reid, G.A. Reduced fibrillar β -amyloid in subcortical structures in a butyrylcholinesterase-knockout Alzheimer disease mouse model. *Chem. Biol. Interact.* **2016**, *259*, 307–312. [[CrossRef](#)]
27. DeBay, D.R.; Reid, G.A.; Macdonald, I.R.; Mawko, G.; Burrell, S.; Martin, E.; Bowen, C.V.; Darvesh, S. Butyrylcholinesterase-knockout reduces fibrillar β -amyloid and conserves 18FDG retention in 5XFAD mouse model of Alzheimer's disease. *Brain Res.* **2017**, *1671*, 102–110. [[CrossRef](#)]
28. Guillozet, A.L.; Mesulam, M.-M.; Smiley, J.F.; Mash, D.C. Butyrylcholinesterase in the life cycle of amyloid plaques. *Ann. Neurol.* **1997**, *42*, 909–918. [[CrossRef](#)]
29. Mesulam, M.; Geula, C. Butyrylcholinesterase reactivity differentiates the amyloid plaques of aging from those of dementia. *Ann. Neurol.* **1994**, *36*, 722–727. [[CrossRef](#)]
30. Ramanan, V.K.; Risacher, S.L.; Nho, K.; Kim, S.; Swaminathan, S.; Shen, L.; Foroud, T.M.; Hakonarson, H.; Huentelman, M.J.; Aisen, P.S.; et al. APOE and BCHE as modulators of cerebral amyloid deposition: A florbetapir PET genome-wide association study. *Mol. Psychiatry* **2014**, *19*, 351–357. [[CrossRef](#)]
31. Reid, G.A.; Darvesh, S. Butyrylcholinesterase-knockout reduces brain deposition of fibrillar β -amyloid in an Alzheimer mouse model. *Neuroscience* **2015**, *298*, 424–435. [[CrossRef](#)]
32. Huang, W.-J.; Zhang, X.; Chen, W.-W. Role of oxidative stress in Alzheimer's disease. *Biomed. Rep.* **2016**, *4*, 519–522. [[CrossRef](#)]
33. Liu, Z.-Q. Bridging free radical chemistry with drug discovery: A promising way for finding novel drugs efficiently. *Eur. J. Med. Chem.* **2020**, *189*, 112020. [[CrossRef](#)]
34. Neha, K.; Haider, M.R.; Pathak, A.; Yar, M.S. Medicinal prospects of antioxidants: A review. *Eur. J. Med. Chem.* **2019**, *178*, 687–704. [[CrossRef](#)]
35. Copley, J.N.; Fiorello, M.L.; Bailey, D.M. 13 reasons why the brain is susceptible to oxidative stress. *Redox Biol.* **2018**, *15*, 490–503. [[CrossRef](#)]
36. Ortiz, G.G.; Pacheco Moises, F.P.; Mireles-Ramirez, M.; Flores-Alvarado, L.J.; Gonzalez-Usigli, H.; Sanchez-Gonzalez, V.J.; Sanchez-Lopez, A.L.; Sanchez-Romero, L.; Diaz-Barba, E.I.; Santoscoy-Gutierrez, J.F.; et al. Oxidative Stress: Love and Hate History in Central Nervous System. *Adv. Protein Chem. Struct. Biol.* **2017**, *108*, 1–31. [[CrossRef](#)]
37. Pohanka, M. Alzheimer's Disease and Oxidative Stress: A Review. *Curr. Med. Chem.* **2013**, *21*, 356–364. [[CrossRef](#)]
38. Pohanka, M. Oxidative stress in Alzheimer disease as a target for therapy. *Bratisl. Med. J.* **2018**, *119*, 535–543. [[CrossRef](#)]
39. Poprac, P.; Jomova, K.; Simunkova, M.; Kollar, V.; Rhodes, C.J.; Valko, M. Targeting Free Radicals in Oxidative Stress-Related Human Diseases. *Trends Pharmacol. Sci.* **2017**, *38*, 592–607. [[CrossRef](#)]
40. Savelieff, M.G.; Nam, G.; Kang, J.; Lee, H.J.; Lee, M.; Lim, M.H. Development of Multifunctional Molecules as Potential Therapeutic Candidates for Alzheimer's Disease, Parkinson's Disease, and Amyotrophic Lateral Sclerosis in the Last Decade. *Chem. Rev.* **2019**, *119*, 1221–1322. [[CrossRef](#)]
41. Guzior, N.; Wieckowska, A.; Panek, D.; Malawska, B. Recent Development of Multifunctional Agents as Potential Drug Candidates for the Treatment of Alzheimer's Disease. *Curr. Med. Chem.* **2014**, *22*, 373–404. [[CrossRef](#)]
42. Makhaeva, G.F.; Kovaleva, N.V.; Rudakova, E.V.; Boltneva, N.P.; Lushchekina, S.V.; Faingold, I.I.; Poletaeva, D.A.; Soldatova, Y.V.; Kotelnikova, R.A.; Serkov, I.V.; et al. New Multifunctional Agents Based on Conjugates of 4-Amino-2,3-polymethylenequinoline and Butylated Hydroxytoluene for Alzheimer's Disease Treatment. *Molecules* **2020**, *25*, 5891. [[CrossRef](#)]
43. Nepovimova, E.; Korabecny, J.; Dolezal, R.; Babkova, K.; Ondrejcek, A.; Jun, D.; Sepsova, V.; Horova, A.; Hrabínova, M.; Soukup, O.; et al. Tacrine-Trolox Hybrids: A Novel Class of Centrally Active, Nonhepatotoxic Multi-Target-Directed Ligands Exerting Anticholinesterase and Antioxidant Activities with Low In Vivo Toxicity. *J. Med. Chem.* **2015**, *58*, 8985–9003. [[CrossRef](#)]

44. Öztaşkın, N.; Çetinkaya, Y.; Taslimi, P.; Göksu, S.; Gülçin, İ. Antioxidant and acetylcholinesterase inhibition properties of novel bromophenol derivatives. *Bioorg. Chem.* **2015**, *60*, 49–57. [[CrossRef](#)]
45. Rosini, M.; Simoni, E.; Bartolini, M.; Tarozzi, A.; Matera, R.; Milelli, A.; Hrelia, P.; Andrisano, V.; Bolognesi, M.L.; Melchiorre, C. Exploiting the lipoic acid structure in the search for novel multitarget ligands against Alzheimer's disease. *Eur. J. Med. Chem.* **2011**, *46*, 5435–5442. [[CrossRef](#)]
46. Li, Y.; Jiao, Q.; Xu, H.; Du, X.; Shi, L.; Jia, F.; Jiang, H. Biometal Dyshomeostasis and Toxic Metal Accumulations in the Development of Alzheimer's Disease. *Front. Mol. Neurosci.* **2017**, *10*, 339. [[CrossRef](#)]
47. Barnham, K.J.; Bush, A.I. Metals in Alzheimer's and Parkinson's Diseases. *Curr. Opin. Chem. Biol.* **2008**, *12*, 222–228. [[CrossRef](#)]
48. Bush, A.I. Drug Development Based on the Metals Hypothesis of Alzheimer's Disease. *J. Alzheimers Dis.* **2008**, *15*, 223–240. [[CrossRef](#)]
49. Huang, X.; Moir, R.D.; Tanzi, R.E.; Bush, A.I.; Rogers, J.T. Redox-Active Metals, Oxidative Stress, and Alzheimer's Disease Pathology. *Ann. N.Y. Acad. Sci.* **2004**, *1012*, 153–163. [[CrossRef](#)]
50. Valko, M.; Jomova, K.; Rhodes, C.J.; Kuča, K.; Musílek, K. Redox- and non-redox-metal-induced formation of free radicals and their role in human disease. *Arch. Toxicol.* **2016**, *90*, 1–37. [[CrossRef](#)]
51. Jomova, K.; Valko, M. Advances in metal-induced oxidative stress and human disease. *Toxicology* **2011**, *283*, 65–87. [[CrossRef](#)] [[PubMed](#)]
52. Xie, S.-S.; Wang, X.-B.; Li, J.-Y.; Yang, L.; Kong, L.-Y. Design, synthesis and evaluation of novel tacrine–coumarin hybrids as multifunctional cholinesterase inhibitors against Alzheimer's disease. *Eur. J. Med. Chem.* **2013**, *64*, 540–553. [[CrossRef](#)] [[PubMed](#)]
53. Agis-Torres, A.; Sollhuber, M.; Fernandez, M.; Sanchez-Montero, J.M. Multi-Target-Directed Ligands and other Therapeutic Strategies in the Search of a Real Solution for Alzheimer's Disease. *Curr. Neuropharmacol.* **2014**, *12*, 2–36. [[CrossRef](#)] [[PubMed](#)]
54. Bachurin, S.O.; Shevtsova, E.F.; Makhaeva, G.F.; Grigoriev, V.V.; Boltneva, N.P.; Kovaleva, N.V.; Lushchekina, S.V.; Shevtsov, P.N.; Neganova, M.E.; Redkozubova, O.M.; et al. Novel conjugates of aminoadamantanes with carbazole derivatives as potential multitarget agents for AD treatment. *Sci. Rep.* **2017**, *7*, 45627. [[CrossRef](#)] [[PubMed](#)]
55. Makhaeva, G.F.; Lushchekina, S.V.; Boltneva, N.P.; Sokolov, V.B.; Grigoriev, V.V.; Serebryakova, O.G.; Vikhareva, E.A.; Aksenenko, A.Y.; Barreto, G.E.; Aliev, G.; et al. Conjugates of γ -Carbolines and Phenothiazine as new selective inhibitors of butyrylcholinesterase and blockers of NMDA receptors for Alzheimer Disease. *Sci. Rep.* **2015**, *5*, 13164. [[CrossRef](#)] [[PubMed](#)]
56. Rosini, M.; Simoni, E.; Minarini, A.; Melchiorre, C. Multi-target Design Strategies in the Context of Alzheimer's Disease: Acetylcholinesterase Inhibition and NMDA Receptor Antagonism as the Driving Forces. *Neurochem. Res.* **2014**, *39*, 1914–1923. [[CrossRef](#)]
57. Simone Tranches Dias, K.; Viegas, C. Multi-Target Directed Drugs: A Modern Approach for Design of New Drugs for the treatment of Alzheimer's Disease. *Curr. Neuropharmacol.* **2014**, *12*, 239–255. [[CrossRef](#)] [[PubMed](#)]
58. Ismaili, L.; Refouvet, B.; Benckekroun, M.; Brogi, S.; Brindisi, M.; Gemma, S.; Campiani, G.; Filipic, S.; Agbaba, D.; Esteban, G.; et al. Multitarget compounds bearing tacrine- and donepezil-like structural and functional motifs for the potential treatment of Alzheimer's disease. *Prog. Neurobiol.* **2017**, *151*, 4–34. [[CrossRef](#)]
59. Korabecny, J.; Spilovska, K.; Mezeiova, E.; Benek, O.; Juza, R.; Kaping, D.; Soukup, O. A Systematic Review on Donepezil-based Derivatives as Potential Cholinesterase Inhibitors for Alzheimer's Disease. *Curr. Med. Chem.* **2019**, *26*, 5625–5648. [[CrossRef](#)]
60. Makhaeva, G.F.; Kovaleva, N.V.; Boltneva, N.P.; Lushchekina, S.V.; Rudakova, E.V.; Stupina, T.S.; Terentiev, A.A.; Serkov, I.V.; Proshin, A.N.; Radchenko, E.V.; et al. Conjugates of tacrine and 1,2,4-thiadiazole derivatives as new potential multifunctional agents for Alzheimer's disease treatment: Synthesis, quantum-chemical characterization, molecular docking, and biological evaluation. *Bioorg. Chem.* **2020**, *94*, 103387. [[CrossRef](#)]
61. Mishra, P.; Kumar, A.; Panda, G. Anti-cholinesterase hybrids as multi-target-directed ligands against Alzheimer's disease (1998–2018). *Bioorg. Med. Chem.* **2019**, *27*, 895–930. [[CrossRef](#)] [[PubMed](#)]
62. Przybyłowska, M.; Dzierzbicka, K.; Kowalski, S.; Chmielewska, K.; Inkielewicz-Stepniak, I. Therapeutic Potential of Multifunctional Derivatives of Cholinesterase Inhibitors. *Curr. Neuropharmacol.* **2021**, *19*, 1323–1344. [[CrossRef](#)]
63. Giacobini, E. Invited Review Cholinesterase inhibitors for Alzheimer's disease therapy: From tacrine to future applications. *Neurochem. Int.* **1998**, *32*, 413–419. [[CrossRef](#)]
64. Knapp, M.J. A 30-Week Randomized Controlled Trial of High-Dose Tacrine in Patients With Alzheimer's Disease. *JAMA* **1994**, *271*, 985–991. [[CrossRef](#)]
65. Milelli, A.; De Simone, A.; Ticchi, N.; Chen, H.H.; Betari, N.; Andrisano, V.; Tumiatti, V. Tacrine-based Multifunctional Agents in Alzheimer's Disease: An Old Story in Continuous Development. *Curr. Med. Chem.* **2017**, *24*, 3522–3546.
66. Spilovska, K.; Korabecny, J.; Nepovimova, E.; Dolezal, R.; Mezeiova, E.; Soukup, O.; Kuca, K. Multitarget Tacrine Hybrids with Neuroprotective Properties to Confront Alzheimer's Disease. *Curr. Top. Med. Chem.* **2017**, *17*, 1006–1026. [[CrossRef](#)] [[PubMed](#)]
67. Makhaeva, G.F.; Kovaleva, N.V.; Boltneva, N.P.; Lushchekina, S.V.; Astakhova, T.Y.; Rudakova, E.V.; Proshin, A.N.; Serkov, I.V.; Radchenko, E.V.; Palyulin, V.A.; et al. New Hybrids of 4-Amino-2,3-polymethylene-quinoline and p-Tolylsulfonamide as Dual Inhibitors of Acetyl- and Butyrylcholinesterase and Potential Multifunctional Agents for Alzheimer's Disease Treatment. *Molecules* **2020**, *25*, 3915. [[CrossRef](#)]
68. Singh, M.; Kaur, M.; Chadha, N.; Silakari, O. Hybrids: A new paradigm to treat Alzheimer's disease. *Mol. Divers.* **2016**, *20*, 271–297. [[CrossRef](#)]
69. Fernández-Bachiller, M.I.; Pérez, C.; González-Muñoz, G.C.; Conde, S.; López, M.G.; Villarroya, M.; García, A.G.; Rodríguez-Franco, M.I. Novel Tacrine–8-Hydroxyquinoline Hybrids as Multifunctional Agents for the Treatment of Alzheimer's Disease, with Neuroprotective, Cholinergic, Antioxidant, and Copper-Complexing Properties. *J. Med. Chem.* **2010**, *53*, 4927–4937. [[CrossRef](#)]

70. Hamulakova, S.; Janovec, L.; Hrabínova, M.; Spilovska, K.; Korabecny, J.; Kristian, P.; Kuca, K.; Imrich, J. Synthesis and Biological Evaluation of Novel Tacrine Derivatives and Tacrine–Coumarin Hybrids as Cholinesterase Inhibitors. *J. Med. Chem.* **2014**, *57*, 7073–7084. [[CrossRef](#)]
71. Xie, S.-S.; Wang, X.; Jiang, N.; Yu, W.; Wang, K.D.G.; Lan, J.-S.; Li, Z.-R.; Kong, L.-Y. Multi-target tacrine-coumarin hybrids: Cholinesterase and monoamine oxidase B inhibition properties against Alzheimer’s disease. *Eur. J. Med. Chem.* **2015**, *95*, 153–165. [[CrossRef](#)]
72. Keri, R.S.; Quintanova, C.; Chaves, S.; Silva, D.F.; Cardoso, S.M.; Santos, M.A. New Tacrine Hybrids with Natural-Based Cysteine Derivatives as Multitargeted Drugs for Potential Treatment of Alzheimer’s Disease. *Chem. Biol. Drug Des.* **2016**, *87*, 101–111. [[CrossRef](#)] [[PubMed](#)]
73. Wang, Y.; Guan, X.-L.; Wu, P.-F.; Wang, C.-M.; Cao, H.; Li, L.; Guo, X.-J.; Wang, F.; Xie, N.; Jiang, F.-C.; et al. Multifunctional Mercapto-tacrine Derivatives for Treatment of Age-Related Neurodegenerative Diseases. *J. Med. Chem.* **2012**, *55*, 3588–3592. [[CrossRef](#)] [[PubMed](#)]
74. Liu, Z.; Fang, L.; Zhang, H.; Gou, S.; Chen, L. Design, synthesis and biological evaluation of multifunctional tacrine-curcumin hybrids as new cholinesterase inhibitors with metal ions-chelating and neuroprotective property. *Bioorg. Med. Chem.* **2017**, *25*, 2387–2398. [[CrossRef](#)] [[PubMed](#)]
75. Minarini, A.; Milelli, A.; Simoni, E.; Rosini, M.; Bolognesi, M.; Marchetti, C.; Tumiatti, V. Multifunctional Tacrine Derivatives in Alzheimer’s Disease. *Curr. Top. Med. Chem.* **2013**, *13*, 1771–1786. [[CrossRef](#)]
76. Przybyłowska, M.; Kowalski, S.; Dzierzbicka, K.; Inkielewicz-Stepniak, I. Therapeutic Potential of Multifunctional Tacrine Analogues. *Curr. Neuropharmacol.* **2019**, *17*, 472–490. [[CrossRef](#)]
77. Sameem, B.; Saeedi, M.; Mahdavi, M.; Shafiee, A. A review on tacrine-based scaffolds as multi-target drugs (MTDLs) for Alzheimer’s disease. *Eur. J. Med. Chem.* **2017**, *128*, 332–345. [[CrossRef](#)] [[PubMed](#)]
78. Tian, S.; Huang, Z.; Meng, Q.; Liu, Z. Multi-Target Drug Design of Anti-Alzheimer’s Disease based on Tacrine. *Mini-Rev. Med. Chem* **2021**, *21*, 2039–2064. [[CrossRef](#)]
79. Makhaeva, G.F.; Lushchekina, S.V.; Boltneva, N.P.; Serebryakova, O.G.; Kovaleva, N.V.; Rudakova, E.V.; Elkina, N.A.; Shchegolkov, E.V.; Burgart, Y.V.; Stupina, T.S.; et al. Novel potent bifunctional carboxylesterase inhibitors based on a polyfluoroalkyl-2-imino-1,3-dione scaffold. *Eur. J. Med. Chem.* **2021**, *218*, 113385. [[CrossRef](#)]
80. Mitchell, A.; Nonhebel, D.C. Spectroscopic studies of tautomeric systems—III. *Tetrahedron* **1979**, *35*, 2013–2019. [[CrossRef](#)]
81. Mao, F.; Huang, L.; Luo, Z.; Liu, A.; Lu, C.; Xie, Z.; Li, X. O-Hydroxyl- or o-amino benzylamine-tacrine hybrids: Multifunctional biometals chelators, antioxidants, and inhibitors of cholinesterase activity and amyloid- β aggregation. *Bioorg. Med. Chem.* **2012**, *20*, 5884–5892. [[CrossRef](#)]
82. Dolomanov, O.V.; Bourhis, L.J.; Gildea, R.J.; Howard, J.A.K.; Puschmann, H. OLEX2: A complete structure solution, refinement and analysis program. *J. Appl. Crystallogr.* **2009**, *42*, 339–341. [[CrossRef](#)]
83. Sheldrick, G.M. SHELXT-Integrated space-group and crystal-structure determination. *Acta Crystallogr. A* **2015**, *71*, 3–8. [[CrossRef](#)] [[PubMed](#)]
84. Sheldrick, G.M. Crystal structure refinement with SHELXL. *Acta Crystallogr. C* **2015**, *71*, 3–8. [[CrossRef](#)] [[PubMed](#)]
85. Taylor, P.; Lappi, S. Interaction of fluorescence probes with acetylcholinesterase. Site and specificity of propidium binding. *Biochemistry* **1975**, *14*, 1989–1997. [[CrossRef](#)] [[PubMed](#)]
86. Re, R.; Pellegrini, N.; Proteggente, A.; Pannala, A.; Yang, M.; Rice-Evans, C. Antioxidant activity applying an improved ABTS radical cation decolorization assay. *Free Radic. Biol. Med.* **1999**, *26*, 1231–1237. [[CrossRef](#)]
87. Makhaeva, G.F.; Elkina, N.A.; Shchegolkov, E.V.; Boltneva, N.P.; Lushchekina, S.V.; Serebryakova, O.G.; Rudakova, E.V.; Kovaleva, N.V.; Radchenko, E.V.; Palyulin, V.A.; et al. Synthesis, molecular docking, and biological evaluation of 3-oxo-2-tolylhydrazinylidene-4,4,4-trifluorobutanoates bearing higher and natural alcohol moieties as new selective carboxylesterase inhibitors. *Bioorg. Chem.* **2019**, *91*, 103097. [[CrossRef](#)]
88. Benzie, I.F.F.; Strain, J.J. The Ferric Reducing Ability of Plasma (FRAP) as a Measure of “Antioxidant Power”: The FRAP Assay. *Anal. Biochem.* **1996**, *239*, 70–76. [[CrossRef](#)]
89. Benzie, I.F.F.; Strain, J.J. Ferric reducing/antioxidant power assay: Direct measure of total antioxidant activity of biological fluids and modified version for simultaneous measurement of total antioxidant power and ascorbic acid concentration. *Methods Enzymol.* **1999**, *299*, 15–27. [[CrossRef](#)]
90. Meir, S.; Kanner, J.; Akiri, B.; Philosoph-Hadas, S. Determination and Involvement of Aqueous Reducing Compounds in Oxidative Defense Systems of Various Senescing Leaves. *J. Agric. Food Chem.* **1995**, *43*, 1813–1819. [[CrossRef](#)]
91. Ferro-Costas, D.; Fernandez-Ramos, A. A Combined Systematic-Stochastic Algorithm for the Conformational Search in Flexible Acyclic Molecules. *Front. Chem.* **2020**, *8*, 16. [[CrossRef](#)]
92. Ferro-Costas, D.; Mosquera-Lois, I.; Fernandez-Ramos, A. TorsiFlex: An automatic generator of torsional conformers. Application to the twenty proteinogenic amino acids. *J. Cheminform.* **2021**, *13*, 100. [[CrossRef](#)] [[PubMed](#)]
93. Frisch, M.J.; Trucks, G.W.; Schlegel, H.B.; Scuseria, G.E.; Robb, M.A.; Cheeseman, J.R.; Scalmani, G.; Barone, V.; Petersson, G.A.; Nakatsuji, H.; et al. *Gaussian 16 Revision C. 01. 2016*; Gaussian Inc.: Wallingford, CT, USA, 2016.
94. Cheung, J.; Rudolph, M.J.; Burshteyn, F.; Cassidy, M.S.; Gary, E.N.; Love, J.; Franklin, M.C.; Height, J.J. Structures of human acetylcholinesterase in complex with pharmacologically important ligands. *J. Med. Chem.* **2012**, *55*, 10282–10286. [[CrossRef](#)] [[PubMed](#)]
95. Nicolet, Y.; Lockridge, O.; Masson, P.; Fontecilla-Camps, J.C.; Nachon, F. Crystal structure of human butyrylcholinesterase and of its complexes with substrate and products. *J. Biol. Chem.* **2003**, *278*, 41141–41147. [[CrossRef](#)]

96. Masson, P.; Lushchekina, S.; Schopfer, L.M.; Lockridge, O. Effects of viscosity and osmotic stress on the reaction of human butyrylcholinesterase with cresyl saligenin phosphate, a toxicant related to aerotoxic syndrome: Kinetic and molecular dynamics studies. *Biochem. J.* **2013**, *454*, 387–399. [CrossRef] [PubMed]
97. Löwdin, P.-O. (Ed.) On the Nonorthogonality Problem. In *Advances in Quantum Chemistry*; Academic Press: Cambridge, MA, USA, 1970; Volume 5, pp. 185–199.
98. Morris, G.M.; Huey, R.; Lindstrom, W.; Sanner, M.F.; Belew, R.K.; Goodsell, D.S.; Olson, A.J. AutoDock4 and AutoDockTools4: Automated docking with selective receptor flexibility. *J. Comput. Chem.* **2009**, *30*, 2785–2791. [CrossRef]
99. Morris, G.M.; Goodsell, D.S.; Halliday, R.S.; Huey, R.; Hart, W.E.; Belew, R.K.; Olson, A.J. Automated docking using a Lamarckian genetic algorithm and an empirical binding free energy function. *J. Comput. Chem.* **1998**, *19*, 1639–1662. [CrossRef]
100. Sushko, I.; Novotarskyi, S.; Körner, R.; Pandey, A.K.; Rupp, M.; Teetz, W.; Brandmaier, S.; Abdelaziz, A.; Prokopenko, V.V.; Tanchuk, V.Y.; et al. Online chemical modeling environment (OCHEM): Web platform for data storage, model development and publishing of chemical information. *J. Comput. Aided Mol. Des.* **2011**, *25*, 533–554. [CrossRef]
101. Radchenko, E.V.; Dyabina, A.S.; Palyulin, V.A.; Zefirov, N.S. Prediction of human intestinal absorption of drug compounds. *Russ. Chem. Bull.* **2016**, *65*, 576–580. [CrossRef]
102. Dyabina, A.S.; Radchenko, E.V.; Palyulin, V.A.; Zefirov, N.S. Prediction of blood-brain barrier permeability of organic compounds. *Dokl. Biochem. Biophys.* **2016**, *470*, 371–374. [CrossRef]
103. Radchenko, E.V.; Dyabina, A.S.; Palyulin, V.A. Towards Deep Neural Network Models for the Prediction of the Blood–Brain Barrier Permeability for Diverse Organic Compounds. *Molecules* **2020**, *25*, 5901. [CrossRef]
104. Radchenko, E.V.; Rulev, Y.A.; Safanyaev, A.Y.; Palyulin, V.A.; Zefirov, N.S. Computer-aided estimation of the hERG-mediated cardiotoxicity risk of potential drug components. *Dokl. Biochem. Biophys.* **2017**, *473*, 128–131. [CrossRef] [PubMed]
105. ADMET Prediction Service. Available online: <http://qsar.chem.msu.ru/admet/> (accessed on 24 June 2022).
106. Bickerton, G.R.; Paolini, G.V.; Besnard, J.; Muresan, S.; Hopkins, A.L. Quantifying the chemical beauty of drugs. *Nat. Chem.* **2012**, *4*, 90–98. [CrossRef] [PubMed]
107. RDKit: Open-Source Cheminformatics Software. Available online: <http://www.rdkit.org> (accessed on 24 June 2022).
108. Šimůnek, P.; Svobodová, M.; Bertolasi, V.; Pretto, L.; Lyčka, A.; Macháček, V. Structure and tautomerism of azo coupling products from N-alkylenaminones derived from acetylacetone and benzoylacetone in solid phase and in solution. *New. J. Chem.* **2007**, *31*, 429–438. [CrossRef]
109. Khudina, O.G.; Shchegol'kov, E.V.; Burgart, Y.V.; Kodess, M.I.; Saloutin, V.I.; Kazheva, O.N.; Shilov, G.V.; D'yachenko, O.A.; Grishina, M.A.; Potemkin, V.A.; et al. Geometric isomerism in the series of fluoroalkyl-containing 1,2,3-trione 2-arylhydrazones. *Russ. J. Org. Chem.* **2007**, *43*, 380–387. [CrossRef]
110. Shchegol'kov, E.V.; Burgart, Y.V.; Saloutin, V.I. The transformations of fluoroalkyl-containing 2-arylhydrazono-1,3-dicarbonyl compounds with methylamine. *J. Fluor. Chem.* **2007**, *128*, 779–788. [CrossRef]
111. Shchegolkov, E.V.; Boltneva, N.P.; Burgart, Y.V.; Lushchekina, S.V.; Serebryakova, O.G.; Elkina, N.A.; Rudakova, E.V.; Perminova, A.N.; Makhaeva, G.F.; Saloutin, V.I. 3-(2-Arylhiazono)-1,1,1-trifluoro-3-(phenylsulfonyl)propan-2-ones as selective carboxylesterase inhibitors. *Russ. Chem. Bull.* **2022**, *71*, 158–164. [CrossRef]
112. Elkina, N.A.; Shchegolkov, E.V.; Burgart, Y.V.; Saloutin, V.I.; Boltneva, N.P.; Serebryakova, O.G.; Lushchekina, S.V.; Makhaeva, G.F. Synthesis of new efficient and selective carboxylesterase inhibitors based on adamantyl and citronellyl 4,4,4-trifluoro-2-arylhydrazonylidene-3-oxobutanoates. *Russ. Chem. Bull.* **2021**, *70*, 567–572. [CrossRef]
113. Makhaeva, G.F.; Radchenko, E.V.; Palyulin, V.A.; Rudakova, E.V.; Aksinenko, A.Y.; Sokolov, V.B.; Zefirov, N.S.; Richardson, R.J. Organophosphorus compound esterase profiles as predictors of therapeutic and toxic effects. *Chem. Biol. Interact.* **2013**, *203*, 231–237. [CrossRef]
114. Makhaeva, G.F.; Rudakova, E.V.; Kovaleva, N.V.; Lushchekina, S.V.; Boltneva, N.P.; Proshin, A.N.; Shchegolkov, E.V.; Burgart, Y.V.; Saloutin, V.I. Cholinesterase and carboxylesterase inhibitors as pharmacological agents. *Russ. Chem. Bull.* **2019**, *68*, 967–984. [CrossRef]
115. Makhaeva, G.F.; Rudakova, E.V.; Serebryakova, O.G.; Aksinenko, A.Y.; Lushchekina, S.V.; Bachurin, S.O.; Richardson, R.J. Esterase profiles of organophosphorus compounds in vitro predict their behavior in vivo. *Chem. Biol. Interact.* **2016**, *259*, 332–342. [CrossRef]
116. Dileep, K.V.; Ihara, K.; Mishima-Tsumagari, C.; Kukimoto-Niino, M.; Yonemochi, M.; Hanada, K.; Shirouzu, M.; Zhang, K.Y.J. Structure of human acetylcholinesterase in complex with tacrine. *PDB* **2021**. [CrossRef]
117. Grishchenko, M.V.; Makhaeva, G.F.; Burgart, Y.V.; Rudakova, E.V.; Boltneva, N.P.; Kovaleva, N.V.; Serebryakova, O.G.; Lushchekina, S.V.; Astakhova, T.Y.; Zhilina, E.F.; et al. Conjugates of Tacrine with Salicylamide as Promising Multitarget Agents for Alzheimer's Disease. *ChemMedChem* **2022**, *17*, e202200080. [CrossRef]
118. Li, P.; Maier, J.M.; Vik, E.C.; Yehl, C.J.; Dial, B.E.; Rickher, A.E.; Smith, M.D.; Pellechia, P.J.; Shimizu, K.D. Stabilizing Fluorine- π Interactions. *Angew. Chem. Int. Ed. Engl.* **2017**, *56*, 7209–7212. [CrossRef] [PubMed]
119. Zueva, I.V.; Lushchekina, S.V.; Pottie, I.R.; Darvesh, S.; Masson, P. 1-(3-Tert-Butylphenyl)-2,2,2-Trifluoroethanone as a Potent Transition-State Analogue Slow-Binding Inhibitor of Human Acetylcholinesterase: Kinetic, MD and QM/MM Studies. *Biomolecules* **2020**, *10*, 1608. [CrossRef] [PubMed]
120. Voevodin, V.; Antonov, A.; Nikitenko, D.; Shvets, P.; Sobolev, S.; Sidorov, I.; Stefanov, K.; Voevodin, V.; Zhumatiy, S. Supercomputer Lomonosov-2: Large scale, deep monitoring and fine analytics for the user community. *Supercomput. Front. Innov.* **2019**, *6*, 4–11. [CrossRef]